# Rectified Brownian movement in molecular and cell biology

Ronald F. Fox
*School of Physics, Georgia Institute of Technology, Atlanta, Georgia 30332-0430*
(Received 19 May 1997; revised manuscript received 18 September 1997)

A unified model is presented for rectified Brownian movement as the mechanism for a variety of putatively chemomechanical energy conversions in molecular and cell biology. The model is established by a detailed analysis of ubiquinone transport in electron transport chains and of allosteric conformation changes in proteins. It is applied to *P*-type ATPase ion transporters and to a variety of rotary arm enzyme complexes. It provides a basis for the dynamics of actin-myosin cross-bridges in muscle fibers. In this model, metabolic free energy does no work directly, but instead biases boundary conditions for thermal diffusion. All work is done by thermal energy, which is harnessed at the expense of metabolic free energy through the establishment of the asymmetric boundary conditions. [S1063-651X(98)13502-X]

PACS number(s): 87.22.−q, 87.10.+e, 05.40.+j

## I. INTRODUCTION

''Brownian movement'' was described for the first time in 1828 by the botanist Brown [1]. He investigated the irregular ''swarming'' motion of all kinds of organic substances, including pollen, dispersed in water. He believed he had found in these particles the ''primitive molecule'' of living matter. Subsequently finding that all sorts of inorganic substances exhibited the same phenomenon, he concluded that all matter was built up of ''primitive molecules'' and that the motion he observed had an inanimate cause. Not quite a century later, the work of Einstein and Perrin [2] clinched this atomistic, or molecular, view of the structure of matter.

During the twentieth century, tremendous advances have been made in the determination of the molecular structures of the consitutents of living matter. It is now clear that Brown's observations can be extended down to the nanometer scale where the Brownian movement of proteins and other molecules can be visualized by light scattering techniques [3]. In fact, it has become clear that the thermal fluctuations in conformation and in translational and rotational motion of macromolecules are the basis for their ''vitality'' after all [4].

In this paper, we will argue that a great many cellular dynamical functions are carried out by proteins undergoing *rectified Brownian movement*. The processes described involve the expenditure of metabolic Gibbs free energy. Often, an image of some sort of direct chemomechanical conversion is mechanistically invoked. Instead, we will argue that each instance of mass motion is exclusively powered by thermal fluctuations, i.e., Brownian movement, but under conditions in which specific boundary conditions have been asymmetrically established at the expense of metabolic energy. Thus metabolic energy does not directly cause concerted motions through some sort of direct chemomechanical energy conversion, but instead *rectifies* an otherwise purely random Brownian movement by modifying boundary conditions. Our case is made for a variety of specific phenomena ranging from the simple translational diffusion of a relatively small molecule [ubiquinone, of molecular weight 862 daltons (d) where 1 d=1 amu] to ion transporters and rotary enzyme complexes. Ultimately, we plan to examine in this way the complex cross-bridge dynamics of complexes of actin and myosin [myosin complex molecular weights are in the hundred millions of daltons for a complex of 500 or so myosin units (each unit is a complex of six polypeptides with a total molecular weight of 540 kd)].

Our perspective is evolutionary. We begin with the early products of evolution associated with the core pathways of energy metabolism and with ion transport and then move towards more recent developments such as in the case of muscle proteins and tubulin proteins. Our objective is to show that evolution has continued to use, in these more complex and recent systems, the basic theme of rectified Brownian movement it established with the earliest systems. While the case for rectified Brownian movement can be made for the simpler cases, there remains debate regarding its applicability to muscle proteins.

The paper is organized as follows. Section II contains an analysis of the role of ubiquinone (or plastoquinone) in the electron transport chains that are responsible for the transduction of reduction-oxidation (redox) energy into the mobile energy currency of adenosine triphosphate (ATP) [5]. Each of these transport chains contains an intermediate step, about a third of the way down the chain, that involves a redox-energy-rectified transmembrane diffusive transport cycle of a quinone species. The quinone cycle produces a coupling of electron flux and proton flux. This is a fundamental example of rectified Brownian movement and provides the foundation for our subsequent analysis. Section III contains an extention of the analysis of the ubiquinone process to the description of protein conformation changes and allostery, fundamental mechanisms of protein function generally. It is shown that such processes can be described as rectified Brownian movement in an abstract conformation state space in which a conformation state potential energy influences the results. This enables us to abstract the fundamental process for application to a wider range of processes. In Sec. IV, this abstract treatment developed for conformation changes is applied to a class of ATPase ion transport mechanisms. These systems provide an especially sharp separation of Brownian movement from the harnessing of metabolic energy to bias boundary conditions. From this perspective, we conclude that the published role of phosphate in

 

*P*-type ATPases is incorrect, in that it cannot be transported across the membrane as part of a chemomechanical conversion, as is often implied. Section V contains an application of this thinking to rotary enzyme complexes. Complexes that incorporate lipoamide, biocytin, and/or phosphopantetheine are described. These examples constitute true cellular rotary nanomotors. In Sec. VI, an analysis of the cross-bridge mechanism of muscle contraction is presented that invokes the rectified Brownian movement paradigm established in the earlier examples. This analysis is in conflict with the ''power stroke'' model. Nevertheless, the objective here is to demonstrate that a consistent model is possible using rectified Brownian movement. We highlight the success of this model with isotonic and auxotonic load-velocity profiles. In Sec. VII, we summarize our findings.

While these examples are sufficient to make the case, several other cases of evolutionarily advanced level systems also exist and have been treated by other authors. These include the *E. coli* flagella motor [6], the kinesin-microtubule system and the dynein-microtubule system [7], and protein translocation across membranes [7]. Indeed, the concept of rectified Brownian movement goes back to Huxley's 1957 model for actin-myosin cross-bridge dynamics [8] and similar mechanisms have been invoked in several other papers [9]. What we attempt to do here is to present an abstracted distillate of the evolutionarily simple mechanisms, which then becomes a unifying framework for the analysis of any of the more advanced and complex cases. Nevertheless, the reader is encouraged to read these other references in which a number of elegant and stimulating specialized results are presented.

The results presented here increase in algebraic complexity as the different cases are analyzed. Even though the fundamental model is easy to describe and understand, the algebraic analysis can be long, even tedious. Nevertheless, each successive case follows from the previous ones as far as the algebraic structure of the results is concerned. Thus there is a common basis to the presentation of the different cases so that we do not have to perform lengthy algebraic calculations over and over again. If the reader keeps this in mind, then the later results will not appear as complicated as they would if viewed in isolation.

## II. UBIQUINONE DIFFUSION

Energy metabolism in all organisms involves the transduction of redox energy into polyphosphate (usually ATP) energy [5,10,11]. Generally, this transduction can take three forms: glycolysis, electron transport, and primary photosynthesis. In glycolysis, a substrate level oxidative phosphorylation occurs that will be of no further interest to us in this paper. In primary photosynthesis, both a photoreduction and a photophosphorylation occur. The products of these two processes are used in secondary photosynthesis to generate sugars from $CO_2$ and $H_2O$, a process that also will be of no further interest to us in this paper. The primary photosynthesis steps involve photosystems I and II, which are coupled by a redox, electron transport chain that includes plastoquinone. This is very closely related to the case we will consider here, which is the case of aerobic electron transport as it occurs in bacterial membranes or in eucaryotic mitochondria inner membranes. In these latter two cases, a key step in the electron transport chain is the participation of ubiquinone (ubi- for ubiquitous), a freely diffusing essential component of the chain. No more will be said here about the photosynthetic case.

Oxidation reactions take three forms: (i) pure one-electron transfers as in the oxidation of iron, $Fe^{2+} \rightarrow Fe^{3+} + e^-$; (ii) two-electron and one-proton transfers as in the oxidation of nicotinamide adenine dinucleotide (NAD), $NADH \rightarrow NAD^+ + 2e^- + H^+$; and (iii) two-electron and two-proton transfers (or one electron and one proton) as in the oxidation of ubiquinone ($UQH_2$), $UQH_2 \rightarrow UQ + 2e^- + 2H^+$. Whenever these oxidations occur, there is always a concomitant reduction of some appropriate acceptor molecule. For example, iron is never elemental in these processes but instead is associated with organic components such as in iron-sulfur proteins or heme-containing proteins (e.g., cytochromes). The organic molecular environment (i.e., the protein component) tunes the redox potential of the iron such that its redox potential ranges from 0.77 (in elemental iron) to $-0.43$ (in ferredoxin). Thus, organically bound iron can be the acceptor for a different organically bound iron oxidation simply by having a higher redox potential than the donor iron. A sequence of appropriately tuned iron-sulfur proteins and cytochromes constitutes the electron transport chains (iron ''wires'' for electric current). High-free-energy electrons are fed into the chains by reduced NADH (redox potential $-0.32$ at $p$H 7), a product of energy metabolism, mostly from the citric acid cycle. They are drawn off at the end of the chain by molecular oxygen $O_2$, which has a redox potential of 0.82 ($p$H 7). A third of the way down this iron-protein chain is a step involving the cyclic reduction and oxidation of $UQH_2$ and UQ.

The quinone step is of interest for several reasons. As far as energy metabolism is concerned, it is of interest because it involves both electrons and protons, whereas the iron proteins involve just electrons. The reduction of the quinone occurs at the inside surface of the membrane (inside the inner mitochondrial membrane or inside a bacterial membrane) and the oxidation occurs on the outside surface of the same membrane. The reduction is driven by electrons supplied by particular iron proteins and the necessary protons are taken up from the interior space enclosed by the membrane. The oxidation is driven by particular iron protein electron acceptors and the protons are freed into the space external to the membrane enclosure. Thus the electron ''current'' has been coupled to a proton current and, moreover, this coupling is ''vectorial'' in that it transports protons from inside to outside the enclosed membrane space. This is the essence of chemiosmosis [5,10–12]. This current-current coupling of electrons and protons energizes the membrane by creating a transmembrane electrochemical potential made up of a combination of pure electric potential difference and a $p$H difference. One of the uses of this energized membrane state is to drive ATP regeneration from degradation products adenosine diphosphate (ADP) and inorganic phosphate ($P_i$) at ATPase protein complexes that are integral parts of the membrane and are driven by the reentry of protons through the ATPase complex into the membrane enclosed space. We will now leave this fascinating part of the energy metabolism story and focus on the step that is of central interest in this paper,

the diffusive shuttling of the quinone back and forth across the membrane.

Ubiquinone is a unique participant in energy metabolism in that it is not bound to a protein. Once reduced on one side of the membrane, $UQH_2$ diffuses in accord with Brownian movement to the other side where it is oxidized to UQ (in mitochondrion there are several complications [10] to this simple picture, simply referred to as the Mitchell cycle, which we will ignore here). UQ then diffuses back to the other side, completing the cycle. In the following, we show that this process is paradigmatic for rectified Brownian movement.

Brownian movement is described by the Langevin equation [13]

$$m\frac{d}{dt}v=-\lambda v+\tilde{F} \tag{1}$$

in which $m$ is the mass of the Brownian particle (molecule), $v$ is its velocity, $\lambda$ is the damping parameter, and $\tilde{F}$ is the fluctuating force caused by the interaction of the fluid molecules with the Brownian particle. The fluctuating force satisfies the fluctuation-dissipation equation

$$\langle\tilde{F}(t)\tilde{F}(t')\rangle=2k_BT\lambda\,\delta(t-t') \tag{2}$$

in which $k_B$ is Boltzmann's constant and $T$ is the temperature. For a spherical particle, we have the Stokes formula

$$\lambda=6\pi\eta R \tag{3}$$

in which $\eta$ is the viscosity of the surrounding fluid and $R$ is the particle's radius. For ubiquinone in the membrane, the viscosity is that of the lipid hydrocarbon side chains of the membrane interior. We will model this environment by lipids with oleate side chains that have a viscosity $\eta=25$ cP at 30 °C. Oleate has one unsaturated carbon-carbon bond, rendering the lipid fluid at this temperature. Ubiquinone (containing ten isoprene units) is a molecule of molecular weight 862 d. It has an aromatic ring head where the redox changes occur and a long isoprenoid tail. In reality, this molecule ''reptates'' through the lipid as it undergoes Brownian movement since its isoprenoid tail is lipophilic, but we will approximate it by a sphere (we are physicists after all) in order to get an order of magnitude feel for its Brownian movement. As a sphere, its radius is about $R=7.5$ Å. The Stokes damping parameter is

$$\lambda=3.5\times10^{-7}\ \text{gm/s}. \tag{4}$$

The Langevin relaxation time $\tau$ is

$$\tau=\frac{m}{\lambda}=3.9\times10^{-15}\ \text{s}. \tag{5}$$

This very short relaxation time suggests that the Langevin process is really in the diffusion limit, which we suspect since we are at very low Reynolds number ($\sim10^{-3}$). The Einstein formula for the diffusion constant $D$ is

$$D=\frac{k_BT}{\lambda}=1.14\times10^{-7}\ \text{cm}^2/\text{s}. \tag{6}$$

This implies that the diffusion time $t_D$, for ubiquinone to traverse the membrane a distance $d$ of about $d=80$ Å is

$$t_D=\frac{d^2}{2D}=2.8\times10^{-6}\ \text{s}. \tag{7}$$

Thus $t_D$ is much greater (nine orders of magnitude) than $\tau$, confirming the validity of the diffusion limit for the Langevin description.

The original stochastic process in Eq. (1) can be recast as a stochastic process equivalent to diffusion by dropping the inertial term, which we have just shown is completely negligible in this case. Writing $v$ as the time derivative of position $x$ yields

$$\frac{d}{dt}x=\frac{\tilde{F}}{\lambda}. \tag{8}$$

Thus we can view this equation, also called a Langevin equation in a generic sense, as describing the stochastic process of the Brownian movement of an ubiquinone molecule through the lipid membrane. Equivalently [i.e., writing the Fokker-Planck equation equivalent to the stochastic equation (8)], we can describe a ubiquinone density as a function of ubiquinone position $f(x,t)$ that satisfies a diffusion equation

$$\frac{\partial}{\partial t}f(x,t)=D\frac{\partial^2}{\partial x^2}f(x,t). \tag{9}$$

In this paper, both perspectives will be invoked.

In physiological steady state, a transmembrane electrochemical potential is established by energy metabolism. The proton-motive potential $\Delta p$ is given by [10,12]

$$\Delta p=\Delta\psi-2.3\frac{RT}{F}\Delta pH, \tag{10}$$

in which $\Delta$ denotes the outside value minus the inside value, $\psi$ is the electric potential, and $F$ is the Faraday constant. A typical value for $\Delta p$ is of order 200 mV [10]. Thus the outward transport of a proton by the ubiquinone cycle is energetically uphill by about $3.2\times10^{-13}$ ergs, or about $8\,k_BT$ at room temperature. The central issue of this paper is the following question: Is redox free energy directly converted into proton kinetic energy in order to get the protons up this transmembrane energy hill, i.e., does it drive them across the membrane? We will argue that the answer to this question is no. Redox free energy is used to asymmetrically bias a diffusion process *by creating asymmetric boundary conditions* at the two membrane surfaces. The diffusion process is simply low Reynolds number Brownian movement and as such is a purely thermal process. Thus thermal energy moves the protons across the membrane, not the redox free energy. Redox free energy provides the means by which thermal energy is harnessed, i.e., rectified, to perform this function.

Our model, the paradigm for all of our models, is a one-dimensional model for transport across the membrane (see Fig. 1). The transmembrane axis is the $x$ axis and the membrane has a thickness $L$ [of order $(80\pm20)$ Å]. At $x=0$ and $L$ there are boundary layers of thickness $\delta$. $\delta$ is the order of

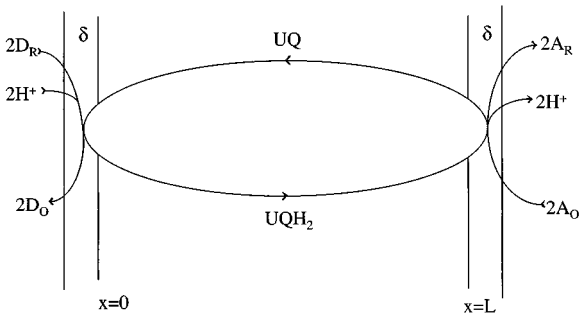


FIG. 1. The membrane thickness extends from $x=0$ to $L$ with boundary layers of thickness $\delta$. The reduced donor $D_R$ and protons $H^+$ combine with ubiquinone (UQ), producing the reduced ubiquinone ($UQH_2$). This molecule diffuses across the membrane where it is reoxidized by an acceptor $A_O$ and releases the protons. The oxidized ubiquinone diffuses back across the membrane, completing the cycle.

a few angstroms. At the $x=0$ boundary layer an electron donor (an iron-sulfur protein, say) $D_R$ supplies electrons while protons are taken up from the interior space. The result is the reduction of UQ to $UQH_2$ and the oxidation of $D_R$ to $D_O$. This reaction takes the form

$$2D_R+2H^++UQ\underset{\alpha_0}{\overset{\beta_0}{\leftrightarrow}}2D_O+UQH_2, \tag{11}$$

in which the forward rate constant is depicted above the arrows and the backward rate constant is depicted below. At the $x=L$ boundary layer an electron acceptor (a cytochrome, say) $A_O$ accepts electrons while protons are given off into the exterior space. The result is the oxidation of $UQH_2$ to UQ and the reduction of $A_O$ to $A_R$. This reaction takes the form

$$2A_O+UQH_2\underset{\beta_L}{\overset{\alpha_L}{\leftrightarrow}}2A_R+2H^++UQ. \tag{12}$$

The standard state (at $p$H 7) redox potential for ubiquinone $E^{0'}_{UQ}$ is 0.10 V. However, at the $x=L$ side of the membrane, the $p$H will be less than 7 because metabolizing bacteria are able to buffer their internal $p$H, thereby maintaining it essentially constant, so that the transport of protons to the outside lowers the external $p$H, making it more acidic [10]. Proton transport also raises the electrical potential, further inhibiting transport. Therefore, we should not use $E^{0'}_{UQ}$ for the external redox potential, but instead should use $E^{0''}_{UQ}$, which must be 0.06 V more positive than $E^{0'}_{UQ}$ for each $p$H unit less than 7 and is increased by adding $\Delta\psi$ as well. The total effect is that $E^{0''}_{UQ}$ is $E^{0'}_{UQ}+\Delta p$, where $\Delta p$ is given by Eq. (10). Thus, if the external $p$H is 6 and $\Delta\psi=0$, say, then $E^{0''}_{UQ}$ is 0.16 V. This means that reaction (12) will tend more to the left with increasing $\Delta p$. No such corrections are necessary for the redox potentials for the iron proteins because iron-dependent redox reactions are independent of $p$H since they are pure electron transfers, not involving protons. Note that, in principle, the width of the membrane influences the results through $\Delta\psi$.

Nominally, it must be true that the standard state redox potential for the donor $E^{0'}_D$ must be less than $E^{0'}_{UQ}$ and the standard state redox potential for the acceptor $E^{0'}_A$ must be greater than $E^{0''}_{UQ}$. However, at a physiological steady state, none of the participating molecular species will be present in standard state concentrations of $1M$. Their molarities are millimolar or less in general. Thus the Gibbs free-energy change associated with Eq. (11) is

$$\Delta G=-2F(E^{0'}_{UQ}-E^{0'}_D)+RT\ \ln\left(\frac{[D_O]^2[UQH_2]}{[D_R]^2[UQ]}\right), \tag{13}$$

where the factor of 2 results from the participation of two electrons in this process and the minus sign reflects their negative charge. Spontaneity of this process requires (the second law of thermodynamics at constant temperature and pressure) that $\Delta G<0$. $E^{0'}_D<E^{0'}_{UQ}$ certainly contributes in this direction, but so does $[D_R]>[D_O]$. Steady-state energy metabolism generates $[D_R]>[D_O]$ and as we will see below, the diffusion process may result in $[UQ]<[UQH_2]$ in the $x=0$ boundary layer. Thus $E^{0'}_D<E^{0'}_{UQ}$ and $[D_R]>[D_O]$ must dominate the possible increase in Gibbs free energy associated with $[UQ]<[UQH_2]$. A parallel analysis at the $x=L$ boundary leads to

$$\Delta G=-2F(E^{0'}_A-E^{0''}_{UQ})+RT\ \ln\left(\frac{[A_R]^2[UQ]}{[A_O]^2[UQH_2]}\right), \tag{14}$$

with the inequalities $E^{0''}_{UQ}<E^{0'}_A$ and $[A_O]>[A_R]$ each supporting $\Delta G<0$ for spontaneity. Steady-state energy metabolism generates $[A_O]>[A_R]$ and as we will see below, the diffusion process may result in $[UQH_2]<[UQ]$ in the $x=L$ boundary layer. Thus $E^{0''}_{UQ}<E^{0'}_A$ and $[A_O]>[A_R]$ must dominate the possible increase in Gibbs free energy associated with $[UQH_2]<[UQ]$. Notice in addition that because $E^{0''}_{UQ}$ is $E^{0'}_{UQ}+\Delta p$, the more positive $\Delta p$ is, the more difficult it is for reaction (12) to proceed to the right. For sufficiently positive $\Delta p$, the spontaneous direction for reaction (12) will be to the left.

Consider a small cross-sectional area of the membrane. Let $X_0$ and $Y_0$ denote the number of $UQH_2$ and UQ molecules, respectively, in the boundary layer at $x=0$ with this cross-sectional area and let $X_L$ and $Y_L$ denote the number of $UQH_2$ and UQ molecules, respectively, in the boundary layer at $x=L$ with the same cross-sectional area. Let $f(x,t)$ denote the density (per unit length for the given cross-sectional area) of $UQH_2$ between $x=0$ and $L$ and let $g(x,t)$ denote the corresponding density for UQ. We have a total quinone $Q$ conservation equation

$$X_0+X_L+\int_0^L dx\ f(x,t)+Y_0+Y_L+\int_0^L dx\ g(x,t)=Q. \tag{15}$$

For $x\in[0,L]$, the densities satisfy the diffusion equations

$$\frac{\partial}{\partial t}f(x,t)=D\ \frac{\partial^2}{\partial x^2}f(x,t), \tag{16}$$

$$\frac{\partial}{\partial t}\, g(x,t) = D\, \frac{\partial^2}{\partial x^2}\, g(x,t), \tag{17}$$

in which we have assumed that the diffusion constant is essentially the same for the oxidized and reduced forms of ubiquinone. Within the layers, we have the mass action equations

$$\frac{d}{dt}\, X_0 = -\alpha_0 X_0 + \beta_0 Y_0 + D\, \frac{\partial}{\partial x}\, f(0,t), \tag{18}$$

$$\frac{d}{dt}\, Y_0 = -\beta_0 Y_0 + \alpha_0 X_0 + D\, \frac{\partial}{\partial x}\, g(0,t), \tag{19}$$

$$\frac{d}{dt}\, X_L = -\alpha_L X_L + \beta_L Y_L - D\, \frac{\partial}{\partial x}\, f(L,t), \tag{20}$$

$$\frac{d}{dt}\, Y_L = -\beta_L Y_L + \alpha_L X_L - D\, \frac{\partial}{\partial x}\, g(L,t), \tag{21}$$

where the suffixes denote which layer is involved. The third term of the right-hand side of each of these equations is the diffusive flux of the relevant species into or out of the boundary layer from the membrane side. In Eqs. (18) and (19) this flux is on the right ($x \geqslant 0$) of the boundary layer and in Eqs. (20) and (21) it is on the left ($x \leqslant L$) of the boundary layer, which accounts for the difference in signs. The boundary conditions that connect Eqs. (16)–(21) are

$$f(0,t) = \frac{X_0}{\delta}, \quad g(0,t) = \frac{Y_0}{\delta}, \qquad f(L,t) = \frac{X_L}{\delta}, \quad g(L,t) = \frac{Y_L}{\delta}. \tag{22}$$

These boundary conditions equate the boundary layer densities with the membrane densities at the boundaries.

The rate constants in Eqs. (18)–(21), $\alpha$ and $\beta$, include the influence of the electron donors and acceptors. For example, consider the reaction in the $x=0$ boundary layer given in Eq. (11). If we leave out the flux term, then this reaction would read

$$\frac{d}{dt}\, X_0 = -a_0 [D_O]^2 X_0 + b_0 [D_R]^2 Y_0, \tag{23}$$

with the rate constant ratio related to the equilibrium constant $K$ by

$$K = \exp\left[ -\frac{\Delta G^{0'}}{RT} \right] = \frac{b_0}{a_0}, \tag{24}$$

where

$$\Delta G^{0'} = -2F(E^{0'}_{\mathrm{UQ}} - E^{0'}_{D}). \tag{25}$$

We have left out the explicit contribution of $H^+$ in Eq. (23) because its effect is absorbed into the standard state (at $p$H 7) redox potentials in Eq. (25) (this is the significance of the primes). Moreover, in Eq. (11), $H^+$ is really $H_3O^+$ and the right-hand, product side should then contain the term $2H_2O$, the effect of which is also absorbed into the standard state redox potentials. Thus the rate constants in Eqs. (11) and (23) are related by

$$\alpha_0 = a_0 [D_O]^2, \quad \beta_0 = b_0 [D_R]^2. \tag{26}$$

If $\Delta G^{0'} \leqslant 0$, then $b_0 \geqslant a_0$, and if energy metabolism maintains $[D_R] > [D_O]$ in the steady state, then $\beta_0 > \alpha_0$. A parallel analysis at the $x=L$ boundary leads to the inequality $\alpha_L > \beta_L$ if energy metabolism maintains $[A_O] > [A_R]$ in the steady state and $\Delta p$ is not too positive. These inequalities manifest the manner by which redox energy affects the boundary conditions for the quinone diffusion.

It is easy to guess the steady-state solution to Eqs. (15)–(22). Using a subscript $S$ to denote the steady state, we find

$$f_S(x) = f_0 - \frac{x}{L}\, (f_0 - f_L), \tag{27}$$

$$g_S(x) = g_0 - \frac{x}{L}\, (g_0 - g_L), \tag{28}$$

in which the constants $f_0$, $f_L$, $g_0$, and $g_L$ satisfy

$$f_0 = \frac{X_{0S}}{\delta}, \quad g_0 = \frac{Y_{0S}}{\delta}, \quad f_L = \frac{X_{LS}}{\delta}, \quad g_L = \frac{Y_{LS}}{\delta}, \tag{29}$$

and

$$X_{0S} + X_{LS} + \frac{L}{2}\, (f_0 + f_L) + Y_{0S} + Y_{LS} + \frac{L}{2}\, (g_0 + g_L) = Q. \tag{30}$$

Substituting Eqs. (27) and (28) into Eqs. (18)–(21) and performing a bit of algebra produces the unique steady-state solutions

$$X_{0S} = \frac{Q\delta}{L + 2\delta}\, \frac{\beta_0(\alpha_L + \beta_L) + r(\beta_0 + \beta_L)}{r(\alpha_0 + \alpha_L + \beta_0 + \beta_L) + (\alpha_0 + \beta_0)(\alpha_L + \beta_L)}, \tag{31}$$

$$Y_{0S} = \frac{Q\delta}{L + 2\delta}\, \frac{\alpha_0(\alpha_L + \beta_L) + r(\alpha_0 + \alpha_L)}{r(\alpha_0 + a_L + \beta_0 + \beta_L) + (\alpha_0 + \beta_0)(\alpha_L + \beta_L)}, \tag{32}$$

$$X_{LS} = \frac{Q\delta}{L + 2\delta}\, \frac{\beta_L(\alpha_0 + \beta_0) + r(\beta_0 + \beta_L)}{r(\alpha_0 + \alpha_L + \beta_0 + \beta_L) + (\alpha_0 + \beta_0)(\alpha_L + \beta_L)}, \tag{33}$$

$$Y_{LS} = \frac{Q\delta}{L + 2\delta}\, \frac{\alpha_L(\alpha_0 + \beta_0) + r(\alpha_0 + \alpha_L)}{r(\alpha_0 + \alpha_L + \beta_0 + \beta_L) + (\alpha_0 + \beta_0)(\alpha_L + \beta_L)}, \tag{34}$$

in which $r$ is an effective diffusive rate defined by

$$r = \frac{D}{L\delta}. \tag{35}$$

From Eq. (6) and the magnitudes of $L$ and $\delta$, it follows that $r$ is of order $10^7\ \mathrm{s}^{-1}$. Generally this is greater than either the $\alpha$'s or the $\beta$'s by several orders of magnitude. This justifies the use of the steady-state solutions. The crucial quantities in

Eqs. (27) and (28), via Eq. (29), are the differences $X_{OS}-X_{LS}$ and $Y_{OS}-Y_{LS}$, in which numerator factors of $r$ drop out:

$$\begin{aligned}-(Y_{0S}-Y_{LS})&=X_{0S}-X_{LS}\\&=\frac{Q\delta}{L+2\delta}\,\frac{\alpha_L\beta_0-\alpha_0\beta_L}{r(\alpha_0+\alpha_L+\beta_0+\beta_L)+(\alpha_0+\beta_0)(\alpha_L+\beta_L)}.\end{aligned}\tag{36}$$

The rate inequalities just below Eq. (26) make it patent that the right-hand side of Eq. (36) is positive. Thus the steady-state profile for $UQH_2$ given by Eq. (27) shows a linear decrease from the $x=0$ side to the $x=L$ side and the steady-state profile for UQ shows the reverse profile, decreasing linearly from $x=L$ to 0. The diffusive fluxes for all $x\in[0,L]$ are given by

$$-D\,\frac{\partial}{\partial x}\,f_S(x)=\frac{D}{L\delta}\,(X_{0S}-X_{LS})>0,\tag{37}$$

$$-D\,\frac{\partial}{\partial x}\,g_S(x)=\frac{D}{L\delta}\,(Y_{0S}-Y_{LS})<0\tag{38}$$

for $UQH_2$ and UQ, respectively.

These fluxes correspond to a mass flow cycle of reduced quinone from $x=0$ to $L$ and of oxidized quinone back from $x=L$ to 0. An important aspect of this process is the change in identity of the quinone from reduced to oxidized and back again. The boundary layer reactions result in a buildup of the reduced species at $x=0$ and a buildup of the oxidized species at $x=L$, so that the separate diffusions create steady-state fluxes as described above. From an individual molecule point of view, it is better to use the stochastic perspective given by Eq. (8). This perspective implies that once a quinone molecule is reduced at $x=0$, it undergoes Brownian movement until it per chance reaches the $x=L$ boundary layer. Once there, there is some chance for it to react, which is another stochastic process, a chemical reaction governed by the rate constants $\alpha_L$ and $\beta_L$. Having changed identity by being oxidized, it undergoes Brownian movement again until per chance it arrives at the $x=0$ boundary layer where the reduction reaction occurs. The reduction too is a stochastic process a chemical reaction governed by the rate constants $\alpha_0$ and $\beta_0$. As long as energy metabolism maintains the rate constant inequalities, this Brownian movement process remains rectified and a net, cyclic flux of quinone mass from $x=0$ to $L$ and back again is maintained. If we set $Q=1$ in Eqs. (15) and (30), then we can interpret the densities $f$ and $g$ as probability densities for the stochastic process we have just described for a single quinone molecule. The diffusion picture provides the steady-state probability density profiles for the stochastic Brownian movement process.

If we turn off energy metabolism, the redox reactions go to equilibrium. This means that the left-hand sides of both Eqs. (13) and (14) vanish. Adding the right-hand sides, exponentiating the sum (which is zero), and using Eqs. (24)–(26) and their parallels at $x=L$, yields

$$1=\frac{\beta_0}{\alpha_0}\,\frac{\alpha_L}{\beta_L}.\tag{39}$$

This means that the differences in Eq. (36) and the fluxes in Eqs. (37) and (38) all vanish. The quinone densities become flat constants for all $x\in[0,L]$.

While energy metabolism is maintained, however, protons are transported across the membrane, uphill energetically, i.e., work is done. The energy of transport is purely thermal and the overcoming of the free-energy barrier for the protons is accomplished by the expenditure of redox energy to bias the boundary conditions for diffusion, by creating strong enough rate constant inequalities in the boundary layers. It should be noted that protons must have some means of reentering the interior space in order to permit a steady state to be maintained. Reentry can be through the ATPase's or through other $H^+$ transporters. The necessity for this consideration is highlighted if we contemplate a bacterium with a volume of one cubic micron. Such a cell has a volume of $10^{-15}$ l. This means that at $p$H 7, it contains $10^{-7}\times6\times10^{23}\times10^{-15}$ unbound protons, which is equal to 60 unbound protons. Obviously, proton reentry is obligatory if a steady state is to be maintained.

The quantity $\Delta p$ may be viewed as the ''load'' against which the quinone cycle must work in order to transport protons across the membrane. The flux given by Eq. (37) may be viewed as proportional to the velocity of the process. Thus it is possible to obtain a ''load-velocity'' curve [7,9(d)] such as have been exhibited for other examples of rectified Brownian movement models. The flux given in Eq. (37) is very well approximated by retaining only the $r$-dependent portion of the denominator given in Eq. (36) because $r$ is much larger than the $\alpha$'s and $\beta$'s, as was noted above. Using Eq. (35) to eliminate the $r$ yields the load-velocity profile formula

$$\begin{aligned}\mathcal{F}=&\frac{Q\delta}{L+2\delta}\\&\times\frac{\beta_0-\alpha_0\,\dfrac{b_L[A_R]^2}{a_L[A_O]^2}\exp\left[\dfrac{2F}{RT}\,(E^{0'}_{\mathrm{UQ}}-E^{0'}_A+\Delta p)\right]}{1+\dfrac{\alpha_0}{\alpha_L}+\dfrac{\beta_0}{\beta_L}+\dfrac{b_L[A_R]^2}{a_L[A_O]^2}\exp\left[\dfrac{2F}{RT}\,(E^{0'}_{\mathrm{UQ}}-E^{0'}_A+\Delta p)\right]}.\end{aligned}\tag{40}$$

If we assume conditions in which all rate constants and concentrations are fixed, except for $\Delta p$, then it is clear that as $\Delta p$ increases, the flux $\mathcal{F}$ decreases until it vanishes when the numerator vanishes. Since $2F/RT$ equals 0.0771 mol/mV at 300 K, the contribution of the $\Delta p$-dependent exponential factor varies from 0 to $5\times10^6$ as $\Delta p$ varies from 0.0 to 200 mV. In this case, a plot of load versus velocity, i.e., $\Delta p$ versus flux, will have a negative first derivative and a positive second derivative, typical of the load-velocity curves for isotonic models of myosin function [9(d)]. In Sec. VI, we show that for muscle we get both isotonic and auxotonic profiles from our model. By scaling both the load and the velocity, these profiles can be compared to universal profiles. The scaling is achieved by dividing $\Delta p$ by the value it has

when it is sufficient to just make the flux vanish and by dividing the flux by the value it has for $\Delta p = 0$.

In the remainder of this paper, we will attempt to show that the mechanism and analysis just presented for ubiquinone can be tailored to a variety of other processes. In each case, we will consider diffusion between boundary layers in which mass action reactions take place.

### III. CONFORMATION CHANGES AND ALLOSTERY

Catalytic proteins, i.e., enzymes, not only recognize their substrates, bind them selectively, catalyze their conversion to products, and release the products, but also interact with various effectors that control protein functionality [5,11]. These effectors are specific molecules recognized by the enzyme and bound to effector sites different from and often remote from the catalytic sites (as much as 20 Å). Effector binding triggers conformation changes in the protein secondary, tertiary, and quarternary structure [4,5]. In some cases, portions of the protein can move up to as much as 15 Å [4,5]. The binding of substrate can also cause such conformation changes and can be responsible for inducing the catalytic activity. Catalysis, in turn, produces bound product that may induce additional conformation changes that then promote product release, after which the enzyme conformation may relax back into the conformation that is poised for selective binding of substrate once again. All of these interactions and induced conformation changes are examples of *allostery*, which literally means ''other shape.'' Nevertheless, the term usually is restricted to the cases in which binding at one site induces a functional change at a different site. Induction of catalytic activity by substrate binding at the catalytic site is called ''induced fit'' instead [14]. In the treatment presented here, each of these different cases will be given a unified description.

Whereas the primary and secondary structures of proteins is determined by the covalently bonded amino acid sequence (which includes cystine disulfide bonds), the tertiary and quarternary structures are determined by weaker bonds including hydrogen bonds, van der Waals bonds, hydrophilic and hydrophobic interactions, and ionic bonds. These weaker bonds are subject to thermal perturbations since their individual strengths are of the order of only several $k_B T$. Thus they fluctuate between being open and closed. Only because several such weak bonds can reinforce each other do they confer any sort of stability to the higher-order structure of the protein. Thus, when one such bond fluctuates open while its neighboring weak bonds remain closed, it is likely that the bond will reclose before all the neighbors also open and allow a large-scale denaturation of the protein. Of course, raising the temperature sufficiently will promote successive openings of several weak bonds and subsequent denaturation. This fact has been put to good use in the related phenomenon of polynucleotide denaturation, wherein it is the first step in the polymerase chain reaction used to clone DNA. The point here is that proteins are dynamic structures constantly exhibiting some degree of thermal fluctuation in their tertiary and quarternary structures [4,15,16]. Under specific conditions, these fluctuations occur around the lowest Gibbs free-energy conformation corresponding to those conditions.

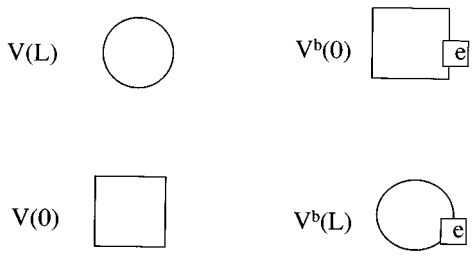


FIG. 2. Shown on the left are the enzyme states $E_1$ and $E_2$ in the absence of the bound effector $e$. The state $E_1$ corresponds to $x = 0$ and the lower potential value $V(0)$. The state $E_2$ corresponds to $x = L$ and the higher potential value $V(L)$. Shown on the right are the enzyme states $eE_1$ and $eE_2$ created by the bound effector $e$. Now the lower potential value is given by $V^b(L)$, while the higher potential value is given by $V^b(0)$.

In the absence of an effector $e$, an enzyme $E$ will fluctuate around its lowest Gibbs free-energy state $E_1$. For definiteness, let us imagine that this state is catalyically inactive and that a higher-energy state $E_2$ is catalytically active. We may abstract this picture by introducing a one-dimensional conformation space coordinate $x$ with $x = 0$ corresponding to the $E_1$ state and $x = L$ corresponding to the $E_2$ state. Unlike the ubiquinone model in which there was no difference in energy between the $x = 0$ and $L$ positions, in this case we associate a conformation potential $V(x)$ with this enzyme and conformation coordinate such that $V(0) < V(L)$ (see Fig. 2). Typically, $V(L) - V(0)$ is at least several times $k_B T$.

The thermal fluctuations of the enzyme, in the absence of the effector, will visit the $x = L$ conformation some of the time. In reaction rate theory [17,18], this is expressed by saying that the ratio of the time $\Delta t$ the enzyme spends within $dx$ of $x$ to some appropriately long time $t$ is given by the Boltzmann formula

$$\frac{\Delta t}{t} = \frac{\exp\left[-\frac{V(x)}{k_B T}\right] dx}{\int_0^L dx \, \exp\left[-\frac{V(x)}{k_B T}\right]}. \tag{41}$$

I will refer to this as *the ergodic interpretation of the canonical Boltzmann distribution*. It has been invoked in reaction rate theory and is the quasi-equilibrium component of activation state theory [17,18]. Its applicability is valid only if fluctuations that bring the enzyme to the conformation $x = L$ result in a reaction of substrate rarely. Thus, in the present case, the enzyme can get to the active conformation by a random thermal fluctuation but not for a sufficiently long enough time for the substrate reaction step to occur with any frequency. What the effector does is stabilize this active conformation so that reaction of substrate does take place with much higher probability. We model this process as follows.

Let the effector bound enzyme state $E_1$ be denoted by $eE_1$, both corresponding to $x = 0$, and let the effector bound enzyme state $E_2$ be denoted by $eE_2$, both corresponding to $x = L$. While the conformation potential for $E_1$ and $E_2$ is $V(x)$, that for $eE_1$ and $eE_2$ will be denoted by $V^b(x)$. The crucial point here is that the binding of the effector alters the

conformation potential and *reverses the stability* so that $V^b(L)<V^b(0)$ (see Fig. 2). A two-step process is envisaged in which the effector binds to the $E_1$ state and then this bound state stochastically and rapidly relaxes into the lowest-free-energy state $eE_2$. It is this state that is the active state of the enzyme. Various possibilities exist for the subsequent steps. The substrate can bind and react as the effector maintains the active state. Substrate binding can occur with the release of the effector, or the substrate can bind, the product can form, and then the effector is released. Examples of almost every variation one can think of are found in cells. We will explore some of them in Sec. IV. When the effector does get released, the enzyme is momentarily in the $E_2$ state and then rapidly relaxes back into the $E_1$ state, in accord with $V(x)$. These steps are represented by the system of reaction equations

$$E_1+e\underset{\alpha_0}{\overset{\beta_0}{\leftrightarrow}}eE_1, \tag{42}$$

$$eE_1\leftrightarrow eE_2, \tag{43}$$

$$eE_2\underset{\beta_L}{\overset{\alpha_L}{\leftrightarrow}}E_2+e, \tag{44}$$

$$E_2\leftrightarrow E_1. \tag{45}$$

We may view reactions (42) and (44) as typical mass action binding and release reactions. Reactions (43) and (45), however, will be viewed as stochastic processes in conformation coordinate space. For reaction relaxation process (45), the stochastic process is the analog of Eq. (8),

$$\frac{d}{dt}\,x=\frac{\widetilde{F}}{\lambda}-\frac{1}{\lambda}\,\frac{d}{dx}\,V(x), \tag{46}$$

in which the fluctuating force satisfies Eq. (2), but where $\lambda$ now denotes an effective damping parameter in conformation coordinate space. This is Brownian movement in the overdamped limit in the presence of a potential. This Langevin equation is equivalent to a Fokker-Planck equation, which in this case is a diffusion equation with a potential-dependent flux. Let $g(x,t)$ denote a probability density for the effector free conformation state. It satisfies the equation

$$\frac{\partial}{\partial t}\,g(x,t)=\frac{\partial}{\partial x}\left(D\,\frac{\partial}{\partial x}+\frac{1}{\lambda}\left[\frac{d}{dx}\,V(x)\right]\right)g(x,t). \tag{47}$$

The boundary conditions for this equation parallel those used in the ubiquinone case. First, we introduce boundary layers in the conformation coordinate space with thickness $\delta$ at $x=0$ and $L$. Second, we denote the densities of $E_2$ in the $x=L$ boundary layer and $E_1$ in the $x=0$ boundary layer, respectively, by $Y_1/\delta$ and $Y_0/\delta$. Similarly, for the reaction relaxation process (43), the stochastic process is also the analog of Eq. (8),

$$\frac{d}{dt}\,x=\frac{\widetilde{F}}{\lambda}-\frac{1}{\lambda}\,\frac{d}{dx}\,V^b(x), \tag{48}$$

with the potential $V^b(x)$. This Langevin equation is equivalent to a Fokker-Planck equation, which in this case is also a diffusion equation with a potential-dependent flux. Let $f(x,t)$ denote a probability density for the effector bound conformation state. It satisfies the equation

$$\frac{\partial}{\partial t}\,f(x,t)=\frac{\partial}{\partial x}\left(D\,\frac{\partial}{\partial x}+\frac{1}{\lambda}\left[\frac{d}{dx}\,V^b(x)\right]\right)f(x,t). \tag{49}$$

We denote the densities of $eE_2$ in the $x=L$ boundary layer and $eE_1$ in the $x=0$ boundary layer, respectively, by $X_L/\delta$ and $X_0/\delta$. Now the boundary conditions for both Eqs. (47) and (49) can be written exactly as in Eq. (22). Steady-state solutions to this system of equations can be expressed in terms of $f_0$, $f_L$, $g_0$, and $g_L$, which satisfy Eq. (29). However, in this case we no longer have the simple solutions (27) and (28), but obtain instead the solutions

$$\begin{aligned}f_S(x)=&f_0\,\exp\left[\frac{V^b(0)-V^b(x)}{\lambda D}\right]\\&+\frac{f_L\,\exp\left[\dfrac{V^b(L)}{\lambda D}\right]-f_0\,\exp\left[\dfrac{V^b(0)}{\lambda D}\right]}{\displaystyle\int_0^L dx\,\exp\left[\frac{V^b(x)}{\lambda D}\right]}\\&\times\exp\left[-\frac{V^b(x)}{\lambda D}\right]\int_0^x dx'\,\exp\left[\frac{V^b(x')}{\lambda D}\right],\end{aligned} \tag{50}$$

$$\begin{aligned}g_S(x)=&g_0\,\exp\left[\frac{V(0)-V(x)}{\lambda D}\right]\\&+\frac{g_L\,\exp\left[\dfrac{V(L)}{\lambda D}\right]-g_0\,\exp\left[\dfrac{V(0)}{\lambda D}\right]}{\displaystyle\int_0^L dx\,\exp\left[\frac{V(x)}{\lambda D}\right]}\\&\times\exp\left[-\frac{V(x)}{\lambda D}\right]\int_0^x dx'\,\exp\left[\frac{V(x')}{\lambda D}\right].\end{aligned} \tag{51}$$

Note that these solutions reduce to the solutions in Eqs. (27) and (28) if the potentials $V$ and $V^b$ are constants. Note also that the Einstein relation (6) implies that each of the exponential factors is a Boltzmann factor because $\lambda D=k_BT$. In the boundary layers, we have the mass action equations paralleling Eqs. (18)–(21). Two important differences must be noted. (i) The diffusive fluxes are now more complicated because of the potentials, as can be seen from Eqs. (47) and (49). (ii) We must interpret the rate constants $\alpha_0$, $\beta_0$, $\alpha_L$, and $\beta_L$ differently from in the ubiquinone case. The result is

$$\begin{aligned}\frac{d}{dt}\,X_0=&-\alpha_0X_0+\beta_0Y_0+D\,\frac{\partial}{\partial x}\,f(0,t)\\&+\frac{1}{\lambda}\left[\frac{d}{dx}\,V^b(0)\right]f(0,t),\end{aligned} \tag{52}$$

$$\frac{d}{dt}\,Y_0 = -\beta_0 Y_0 + \alpha_0 X_0 + D\,\frac{\partial}{\partial x}\,g(0,t) + \frac{1}{\lambda}\left[\frac{d}{dx}\,V(0)\right]g(0,t), \tag{53}$$

$$\frac{d}{dt}\,X_L = -\alpha_L X_L + \beta_L Y_L - D\,\frac{\partial}{\partial x}\,f(L,t) - \frac{1}{\lambda}\left[\frac{d}{dx}\,V^b(L)\right]f(L,t), \tag{54}$$

$$\frac{d}{dt}\,Y_L = -\beta_L Y_L + \alpha_L X_L - D\,\frac{\partial}{\partial x}\,g(L,t) - \frac{1}{\lambda}\left[\frac{d}{dx}\,V(L)\right]g(L,t). \tag{55}$$

In the present case, both $\beta_0$ and $\beta_L$ are proportional to $[e]$, the effector concentration, whereas $\alpha_0$ and $\alpha_L$ are not. This is to be contrasted with Eq. (26). Denote the standard state Gibbs free-energy change for reaction (42) by $\Delta G_1^0$ and that for reaction (44) by $\Delta G_2^0$. The equilibrium constants for these reactions, $K_1$ and $K_2$, respectively, satisfy

$$K_1 = \exp\left[-\frac{\Delta G_1^0}{k_B T}\right] = \frac{\beta_0}{\alpha_0}, \quad K_2 = \exp\left[-\frac{\Delta G_2^0}{k_B T}\right] = \frac{\alpha_L}{\beta_L}. \tag{56}$$

Stabilization of the activated state is caused by $\Delta G_1^0 < 0$ and $\Delta G_2^0 > 0$ for sufficiently large $[e]$. The first inequality favors binding of the effector $e$ to the $E_1$ state of the enzyme, while the second inequality favors maintenance of the $eE_2$ state. We see from Eq. (56) that these inequalities imply $\beta_0 > \alpha_0$ and $\beta_L > \alpha_L$. Generally, the absolute rate of effector binding $\beta_0$ will be greater than the absolute rate of release $\alpha_L$.

Equations (47) and (49) may be used to show that Eqs. (52)–(55) are consistent with the total enzyme conservation law [cf. Eq. (15)]

$$X_0 + X_L + \int_0^L dx\; f(x,t) + Y_0 + Y_L + \int_0^L dx\; g(x,t) = E, \tag{57}$$

where $E$ denotes the total amount of enzyme in all possible states. The probability interpretation of the densities corresponds to setting $E = 1$.

The presence of the potential terms makes the algebra for the steady-state solution more complicated than it was in the ubiquinone section. In order to facilitate matters, we introduce a shorthand notation

$$e_0 = \exp\left[\frac{V(0)}{\lambda D}\right], \quad e_L = \exp\left[\frac{V(L)}{\lambda D}\right], \quad e_0^b = \exp\left[\frac{V^b(0)}{\lambda D}\right], \quad e_L^b = \exp\left[\frac{V^b(L)}{\lambda D}\right]; \tag{58}$$

$$N = \int_0^L dx\; \exp\left[\frac{V(x)}{\lambda D}\right], \quad N^b = \int_0^L dx\; \exp\left[\frac{V^b(x)}{\lambda D}\right]; \tag{59}$$

$$I = e_0 \int_0^L dx\; \exp\left[-\frac{V(x)}{\lambda D}\right], \quad I^b = e_0^b \int_0^L dx\; \exp\left[-\frac{V^b(x)}{\lambda D}\right]; \tag{60}$$

$$J = \int_0^L dx\; \exp\left[-\frac{V(x)}{\lambda D}\right]\int_0^x dx' \exp\left[\frac{V(x')}{\lambda D}\right], \quad J^b = \int_0^L dx\; \exp\left[-\frac{V^b(x)}{\lambda D}\right]\int_0^x dx' \exp\left[\frac{V^b(x')}{\lambda D}\right]; \tag{61}$$

$$r = \frac{D}{N\delta}, \quad r^b = \frac{D}{N^b\delta}. \tag{62}$$

With these definitions, the steady-state versions of Eqs. (50)–(55) and (57) become

$$-\alpha_0 X_{0S} + \beta_0 Y_{0S} + r^b(X_{LS} e_L^b - X_{0S} e_0^b) = 0, \tag{63}$$

$$-\beta_0 Y_{0S} + \alpha_0 X_{0S} + r(Y_{LS} e_L - Y_{0S} e_0) = 0, \tag{64}$$

$$-\alpha_L X_{LS} + \beta_L Y_{LS} - r^b(X_{LS} e_L^b - X_{0S} e_0^b) = 0, \tag{65}$$

$$-\beta_L Y_{LS} + \alpha_L X_{LS} - r(Y_{LS} e_L - Y_{0S} e_0) = 0, \tag{66}$$

$$X_{0S} + X_{LS} + X_{0S}\,\frac{I^b}{\delta} + \frac{J^b}{N^b\delta}\,(X_{LS} e_L^b - X_{0S} e_0^b) + Y_{0S} + Y_{LS} + Y_{0S}\,\frac{I}{\delta} + \frac{J}{N\delta}\,(Y_{LS} e_L - Y_{0S} e_0) = E. \tag{67}$$

The solutions to these equations are

$$Y_{LS} = \frac{(\alpha_0 e_0 r + \beta_0 e_0^b r^b)\alpha_L + (\alpha_0 e_L^b + \alpha_L e_0^b) e_0 r r^b}{(\alpha_0 e_0 r + \beta_0 e_0^b r^b)\beta_L + (\beta_0 e_L + \beta_L e_0) e_0^b r r^b}\,X_{LS}, \tag{68}$$

$$Y_{0S} = \frac{(\alpha_L e_L r + \beta_L e_L^b r^b)\alpha_0 + (\alpha_0 e_L^b + \alpha_L e_0^b) e_L r r^b}{(\alpha_0 e_0 r + \beta_0 e_0^b r^b)\beta_L + (\beta_0 e_L + \beta_L e_0) e_0^b r r^b}\,X_{LS}, \tag{69}$$

$$X_{0S} = \frac{(\beta_0 + e_0 r)\beta_L e_L^b r^b + (\alpha_L + e_L^b r^b)\beta_0 e_L r}{(\alpha_0 e_0 r + \beta_0 e_0^b r^b)\beta_L + (\beta_0 e_L + \beta_L e_0) e_0^b r r^b}\,X_{LS}, \tag{70}$$

$$\begin{aligned} E = {} & [(\alpha_0 e_0 r + \beta_0 e_0^b r^b)\beta_L + (\beta_0 e_L + \beta_L e_0) e_0^b r r^b]^{-1} \\ & \times \Big\{ [\alpha_0\beta_L(e_0 r + e_L^b r^b) + \alpha_L\beta_0(e_0^b r^b + e_L r) \\ & + (\alpha_0\alpha_L + \alpha_0 e_L^b r^b + \alpha_L e_0^b r^b)(e_0 + e_L) r \\ & + (\beta_0\beta_L + \beta_0 e_L r + \beta_L e_0 r)(e_0^b + e_L^b) r^b] \\ & + \frac{I^b}{\delta}\,[(\beta_0 + e_0 r)\beta_L e_L^b r^b + (\alpha_L + e_L^b r^b)\beta_0 e_L r] \\ & + \frac{I}{\delta}\,[(\alpha_0 + e_0^b r^b)\alpha_L e_L r + (\beta_L + e_L r)\alpha_0 e_L^b r^b] \end{aligned}$$

$$+\frac{J^b-J}{\delta}\frac{D}{N^bN\delta}(\alpha_0\beta_Le_0e_L^b-\alpha_L\beta_0e_Le_0^b)\Bigg\}X_{LS}. \tag{71}$$

Given $E$, we invert Eq. (71) to get $X_{LS}$ and then substitute it into Eqs. (68)–(70) to obtain explicit solutions.

The significance of these results is that they show how the binding of effector $e$ leads to an increased steady-state value of the reactive enzyme state, which is $E_2$ in the absence of effector and $eE_2$ in its presence. In the absence of effector, only reaction equation (45) is operative. In equilibrium, the proportion of enzyme molecules within $dx$ of $x=0$ is given by ($dx$ of order $\delta$ corresponds to the boundary layers)

$$P(E_1)dx=\frac{\int_0^{dx}dx'\ \exp\left[-\frac{V(x')}{k_BT}\right]}{\int_0^L dx\ \exp\left[-\frac{V(x)}{k_BT}\right]}$$

$$\cong\frac{dx\ \exp\left[-\frac{V(0)}{k_BT}\right]}{\int_0^L dx\ \exp\left[-\frac{V(x)}{k_BT}\right]}=\frac{dx}{I} \tag{72}$$

and the proportion within $dx$ of $x=L$ is given by

$$P(E_2)dx=\frac{\int_{L-dx}^{L}dx'\ \exp\left[-\frac{V(x')}{k_BT}\right]}{\int_0^L dx\exp\left[-\frac{V(x)}{k_BT}\right]}$$

$$\cong\frac{dx\ \exp\left[-\frac{V(L)}{k_BT}\right]}{\int_0^L dx\ \exp\left[-\frac{V(x)}{k_BT}\right]}=\frac{dx\ e_0}{I\ e_L}. \tag{73}$$

Because $V(L)-V(0)$ is typically several times $k_BT$, the fraction of enzyme in the active state satisfies

$$\frac{P(E_2)}{P(E_1)}\cong\frac{e_0}{e_L}\ll 1. \tag{74}$$

In the presence of effector $e$, however, all four reaction equations (42)–(45) are operative. The reactive enzyme state is $eE_2$ and the ratio of the amount of this to the amount of unreactive enzyme in state $E_1$ is given by

$$\frac{X_{LS}}{Y_{0S}}=\frac{(\alpha_0e_0r+\beta_0e_0^br^b)\beta_L+(\beta_0e_L+\beta_Le_0)e_0^brr^b}{(\alpha_Le_Lr+\beta_Le_L^br^b)\alpha_0+(\alpha_0e_L^b+\alpha_Le_0^b)e_Lrr^b}, \tag{75}$$

as follows directly from Eq. (69). Since the $\beta$'s are proportional to $[e]$ and the $\alpha$'s are not, it is clear that this ratio vanishes when $[e]=0$ and increases with increasing $[e]$. Note that the right-hand side of Eq. (74) is reproduced by the ratio $Y_{LS}/Y_{0S}$ given by Eqs. (68) and (69) when $[e]=0$ (take the ratio before setting $[e]=0$). For sufficiently large $[e]$ and because the effective diffusive rates $r$ and $r^b$ are generally a few orders of magnitude larger than the $\alpha$'s and $\beta$'s, we have, using the inequalities beneath Eq. (56),

$$\frac{X_{LS}}{Y_{0S}}\cong\frac{\beta_0e_0^b}{\alpha_0e_L^b+\alpha_Le_0^b}>1. \tag{76}$$

Comparison with Eq. (74) confirms that the active state of the enzyme is much more likely if sufficient effector is present. A parallel argument could be made wherein the binding of the effector inactivated an active enzyme instead. Other variations are possible. In the next section, we focus on a mechanism in which effector binding transforms the enzyme to the active state, but subsequent substrate binding promotes release of effector. This will lead to a cyclic process akin to the ubiquinone cycle.

## IV. *P*-TYPE ION CHANNEL ATPASES

ATP-driven active transport is prevalent in organisms. Transport of potassium, sodium, calcium, and protons against concentration gradients is mediated by this class of transporters that contain ATPase activity. They utilize the Gibbs free energy of ATP to perform their function. As we shall see, the energy of ATP is not directly converted into ion energy and does not drive the ions across the membrane. Instead, this energy is used to promote allosteric conformation changes that amount to a biasing of boundary conditions for Brownian movement in conformation state space (see the preceding section). In this paper, we restrict attention to *P*-type ATPases that are usually found in the plasma membrane. These ATPases are modeled as having two conformation states $E_1$ and $E_2$, between which allosterically induced shifts are caused by phosphorylation and dephosphorylation of a particular aspartate residue [5,19].

The $\beta$-carboxyl side chain of an essential aspartate is phosphorylated. This aspartyl phosphate is a very-high-energy phosphate, with a free energy of hydrolysis standard state value of $\Delta G^{o'}=-13$ kcal/mol [20]. This is nearly twice the value for ATP hydrolysis at a standard state ($-7.3$ kcal/mol), so that a favorable degree of phosphorylation requires a high ratio of [ATP] to [ADP] and $[P_i]$, i.e., an active physiological ATP state. More importantly, it is clear that the free energy of ATP has not gone into the energy of the ions since it has been conserved by the high-energy aspartyl phosphate. What is going on here is a phosphorylation designed to cause a conformation change. Upon dephosphorylation, the conformation will shift back to its original state. While hydrolysis of the aspartyl phosphate does release considerable free energy, this energy is not directly converted into ion energy but instead renders the dephosphorylation step nearly irreversible, thereby considerably biasing the boundary conditions for Brownian movement. In the case of the calcium ATPase, this is especially apparent since the calcium ion transport across the membrane is over before the aspartyl phosphate is hydrolyzed. In the case of the sodium-potassium antiporter, the sodium transport is finished before the aspartyl phosphate is hydrolyzed, and while hydrolysis is concomitant with the potassium transport, it is the conformation change in the ATPase that translocates the potassium, not the energy released by phosphate hydrolysis. Very similar considerations of con-

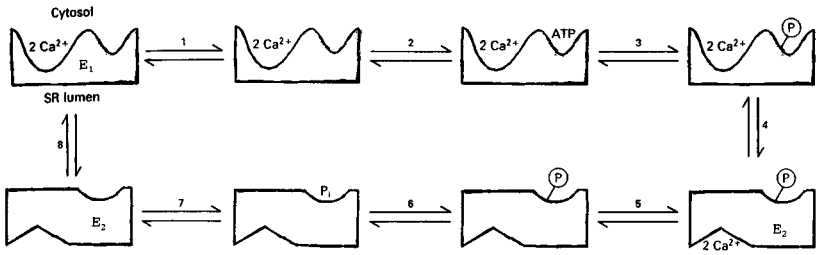


FIG. 3. The calcium ATPase in state $E_1$ binds calcium from the cytosol side of the membrane (1). ATP is subsequently bound (2) and a phosphorylation of an aspartate residue occurs (3). This induces a conformation change that everts the calcium binding site to the opposite side of the membrane (4), creating enzyme state $E_2$. Calcium is released (5), dephosphorylation ensues (6 and 7), and eversion of the calcium binding site back to the cytolsol side (8) completes the cycle.

servation of high-free-energy phosphate bonds and conformation change upon phosphorylation or dephosphorylation as opposed to direct chemomechanical conversion have been broached in the context of ATP myosin interactions in muscle fibers [21], to which we will return later.

We model the calcium ATPase first (see Fig. 3). The $E_1$ state of the enzyme has a calcium binding site open to the cytosol side of the membrane, i.e., the space enclosed by the plasma membrane. There is also an $E_2$ state with the calcium binding site open to the exterior. In the absence of phosphorylation, the $E_1$ state is the lowest-free-energy state and the $E_2$ state is a higher-free-energy state, fluctuations to which are rare. The $E_1$ binding state binds two divalent $Ca^{2+}$ ions. The ion bound $E_1$ state $CaE_1$ then binds ATP. Aspartate phosphorylation ensues, creating the $CaE_1$-$P$ state. This state exhibits reversed stability and is higher in free energy than the state $CaE_2$-$P$, to which it relaxes rapidly. This relaxation includes an eversion of the $Ca^{2+}$ binding site from inside to outside, as well as a decrease in binding affinity for $Ca^{2+}$. Thus release of calcium ion is to the outside and membrane transport is completed. The $CaE_2$-$P$ state releases bound $Ca^{2+}$, becoming $E_2$-$P$, and is readily dephosphorylated to the $E_2$ state, which then rapidly relaxes to the $E_1$ state, completing the enzyme state cycle. The allosteric nature of this cycle is underscored by the necessity for the site of the calcium eversion to be distinct from the aspartate site, so that phosphate always remains on the cytosol side of the membrane and is not also transported.

As in Sec. III, we may describe the relative stabilities of $CaE_1$ and $CaE_2$ in terms of a potential $V(x)$ and the relative stabilities of $CaE_1$-$P$ and $CaE_2$-$P$ in terms of a potential $V^b(x)$, each with respect to a conformation state space variable $x$. Clearly, $CaE_1$-$P$ and $CaE_2$-$P$ are the analogs of $eE_1$ and $eE_2$, respectively. The analogs to Eqs. (42)–(45) become

$$2\mathrm{Ca}^{2+}+E_1 \underset{\nu_0}{\overset{\mu_0}{\leftrightarrow}} \mathrm{Ca}E_1, \tag{77}$$

$$\mathrm{ATP}+\mathrm{Ca}E_1 \underset{\alpha_0}{\overset{\beta_0}{\leftrightarrow}} \mathrm{Ca}E_1-P+\mathrm{ADP}, \tag{78}$$

$$\mathrm{Ca}E_1-P \leftrightarrow \mathrm{Ca}E_2-P, \tag{79}$$

$$\mathrm{Ca}E_2-P \underset{\beta_L}{\overset{\alpha_L}{\leftrightarrow}} E_2-P+2\mathrm{Ca}^{2+}, \tag{80}$$

$$E_2-P \underset{\mu_L}{\overset{\nu_L}{\leftrightarrow}} E_2+P_i, \tag{81}$$

$$E_2 \leftrightarrow E_1. \tag{82}$$

We may view reactions (77), (78), (80), and (81) as typical mass action reactions. Reactions (79) and (82), however, will be viewed as stochastic processes in conformation coordinate space.

The parallel with Sec. III is only partial. Equations (42)–(45) are now Eqs. (78), (79), (81), and (82) and there is an additional pair of equations (77) and (80) that involves calcium binding and release. The variables $X_0$, $X_L$, $Y_0$, and $Y_L$ of Sec. III are now associated with $CaE_1$-$P$, $CaE_2$-$P$, $E_1$, and $E_2$, respectively. In addition, we associate the new variables $Z_0$ and $Z_L$ with $CaE_1$ and $E_2$-$P$, respectively. Once again, we introduce boundary layers in the conformation coordinate space. Thus much of the analysis in Sec. III can be carried over into this section.

The diffusion equations (47) and (49) and their steady-state solutions (50) and (51) take precisely the same form here. However, Eqs. (52)–(55) become

$$\frac{d}{dt}X_0 = -\alpha_0 X_0+\beta_0 Z_0+D\frac{\partial}{\partial x}f(0,t) + \frac{1}{\lambda}\left[\frac{d}{dx}V^b(0)\right]f(0,t), \tag{83}$$

$$\frac{d}{dt}Y_0 = -\mu_0 Y_0+\nu_0 Z_0+D\frac{\partial}{\partial x}g(0,t)+\frac{1}{\lambda}\left[\frac{d}{dx}V(0)\right]g(0,t), \tag{84}$$

$$\frac{d}{dt}Z_0 = \mu_0 Y_0-\nu_0 Z_0-\beta_0 Z_0+\alpha_0 X_0, \tag{85}$$

$$\frac{d}{dt}X_L = -\alpha_L X_L+\beta_L Z_L-D\frac{\partial}{\partial x}f(L,t) - \frac{1}{\lambda}\left[\frac{d}{dx}V^b(L)\right]f(L,t), \tag{86}$$

$$\frac{d}{dt}\,Y_L=-\mu_L Y_L+\nu_L Z_L-D\,\frac{\partial}{\partial x}\,g(L,t)$$

$$-\frac{1}{\lambda}\left[\frac{d}{dx}\,V(L)\right]g(L,t), \tag{87}$$

$$\frac{d}{dt}\,Z_L=\mu_L Y_L-\nu_L Z_L-\beta_L Z_L+\alpha_L X_L\,. \tag{88}$$

The rate constants here have different interpretations than they did in Sec. III. Here $\alpha_0$ is proportional to [ADP], $\beta_0$ is proportional to [ATP], $\mu_0$ is proportional to $[Ca^{2+}]^2$ at $x=0$, $\beta_L$ is proportional to $[Ca^{2+}]$ at $x=L$, and $\mu_L$ is proportional to $[P_i]$. In general, each of these concentrations will also change with time as a result of their involvement in Eqs. (83)–(88). However, they will also change in accord with other physiological processes independent of the transport process we are describing. Thus we will assume that each of these concentrations is maintained at some physiological steady-state value by these other processes and focus our attention exclusively on the Ca-ATPase enzyme conformation dynamics.

From Eqs. (50) and (51), the steady-state fluxes for all $x\varepsilon[0,L]$ are found to be given by [cf. Eqs. (37) and (38)]

$$-D\,\frac{\partial}{\partial x}\,f_S(x)-\frac{1}{\lambda}\left[\frac{d}{dx}\,V^b(x)\right]f_S(x)=-r^b(X_{LS}e_L^b-X_{0S}e_0^b), \tag{89}$$

$$-D\,\frac{\partial}{\partial x}\,g_S(x)-\frac{1}{\lambda}\left[\frac{d}{dx}\,V(x)\right]g_S(x)=-r(Y_{LS}e_L-Y_{0S}e_0). \tag{90}$$

The steady-state equations (63)–(67) become

$$-\alpha_0 X_{0S}+\beta_0 Z_{0S}+r^b(X_{LS}e_L^b-X_{0S}e_0^b)=0, \tag{91}$$

$$-\mu_0 Y_{0S}+\nu_0 Z_{0S}+r(Y_{LS}e_L-Y_{0S}e_0)=0, \tag{92}$$

$$\mu_0 Y_{0S}-\nu_0 Z_{0S}-\beta_0 Z_{0S}+\alpha_0 X_{0S}=0, \tag{93}$$

$$-\alpha_L X_{LS}+\beta_L Z_{LS}-r^b(X_{LS}e_L^b-X_{0S}e_0^b)=0, \tag{94}$$

$$-\mu_L Y_{LS}+\nu_L Z_{LS}-r(Y_{LS}e_L-Y_{0S}e_0)=0, \tag{95}$$

$$\mu_L Y_{LS}-\nu_L Z_{LS}-\beta_L Z_{LS}+\alpha_L X_{LS}=0, \tag{96}$$

$$X_{0S}+Y_{0S}+Z_{0S}+X_{0S}\,\frac{I^b}{\delta}+\frac{J^b}{N^b\delta}\,(X_{LS}e_L^b-X_{0S}e_0^b)+X_{LS}$$

$$+Y_{LS}+Z_{LS}+Y_{0S}\,\frac{I}{\delta}+\frac{J}{N\delta}\,(Y_{LS}e_L-Y_{0S}e_0)=E. \tag{97}$$

Equations (93) and (96) have simple solutions given by

$$Z_{0S}=\frac{\alpha_0 X_{0S}+\mu_0 Y_{0S}}{\beta_0+\nu_0}, \tag{98}$$

$$Z_{LS}=\frac{\alpha_L X_{LS}+\mu_L Y_{LS}}{\beta_L+\nu_L}. \tag{99}$$

When these are substituted into Eqs. (91), (92), (94), and (95), we obtain Eqs. (63)–(66) with the $\alpha$'s and $\beta$'s of Eqs. (63)–(66) replaced by $\overline{\alpha}$'s and $\overline{\beta}$'s defined by

$$\overline{\alpha_0}=\frac{\nu_0}{\beta_0+\nu_0}\,\alpha_0,\quad \overline{\alpha_L}=\frac{\nu_L}{\beta_L+\nu_L}\,\alpha_L,$$

$$\overline{\beta_0}=\frac{\mu_0}{\beta_0+\nu_0}\,\beta_0,\quad \overline{\beta_L}=\frac{\mu_L}{\beta_L+\nu_L}\,\beta_L. \tag{100}$$

This means that the solutions in Eqs. (68)–(70) also provide the steady-state solutions we seek here by simple substitutions

$$Y_{LS}=\frac{(\overline{\alpha_0}e_0 r+\overline{\beta_0}e_0^b r^b)\overline{\alpha_L}+(\overline{\alpha_0}e_L^b+\overline{\alpha_L}e_0^b)e_0 r r^b}{(\overline{\alpha_0}e_0 r+\overline{\beta_0}e_0^b r^b)\overline{\beta_L}+(\overline{\beta_0}e_L+\overline{\beta_L}e_0)e_0^b r r^b}\,X_{LS}, \tag{101}$$

$$Y_{0S}=\frac{(\overline{\alpha_L}e_L r+\overline{\beta_L}e_L^b r^b)\overline{\alpha_0}+(\overline{\alpha_0}e_L^b+\overline{\alpha_L}e_0^b)e_L r r^b}{(\overline{\alpha_0}e_0 r+\overline{\beta_0}e_0^b r^b)\overline{\beta_L}+(\overline{\beta_0}e_L+\overline{\beta_L}e_0)e_0^b r r^b}\,X_{LS}, \tag{102}$$

$$X_{0S}=\frac{(\overline{\beta_0}+e_0 r)\overline{\beta_L}e_L^b r^b+(\overline{\alpha_L}+e_L^b r^b)\overline{\beta_0}e_L r}{(\overline{\alpha_0}e_0 r+\overline{\beta_0}e_0^b r^b)\overline{\beta_L}+(\overline{\beta_0}e_L+\overline{\beta_L}e_0)e_0^b r r^b}\,X_{LS}. \tag{103}$$

Equation (71), however, does not go over so simply because of the extra, $Z$-dependent terms in Eq. (97). Instead, we obtain

$$E=[(\overline{\alpha_0}e_0 r+\overline{\beta_0}e_0^b r^b)\overline{\beta_L}+(\overline{\beta_0}e_L+\overline{\beta_L}e_0)e_0^b r r^b]^{-1}\left\{\left(1+\frac{\alpha_L}{\beta_L+\nu_L}\right)[(\overline{\alpha_0}e_0 r+\overline{\beta_0}e_0^b r^b)\overline{\beta_L}+(\overline{\beta_0}e_L+\overline{\beta_L}e_0)e_0^b r r^b]\right.$$

$$+\left(1+\frac{\alpha_0}{\beta_0+\nu_0}\right)[(\overline{\beta_0}+e_0 r)\overline{\beta_L}e_L^b r^b+(\overline{\alpha_L}+e_L^b r^b)\overline{\beta_0}e_L r]+\left(1+\frac{\mu_0}{\beta_0+\nu_0}\right)[(\overline{\alpha_L}e_L r+\overline{\beta_L}e_L^b r^b)\overline{\alpha_0}+(\overline{\alpha_0}e_L^b+\overline{\alpha_L}e_0^b)e_L r r^b]$$

$$+\left(1+\frac{\mu_L}{\beta_L+\nu_L}\right)[(\overline{\alpha_0}e_0 r+\overline{\beta_0}e_0^b r^b)\overline{\alpha_L}+(\overline{\alpha_0}e_L^b+\overline{\alpha_L}e_0^b)e_0 r r^b]+\frac{I^b}{\delta}[(\overline{\beta_0}+e_0 r)\overline{\beta_L}e_L^b r^b+(\overline{\alpha_L}+e_L^b r^b)\overline{\beta_0}e_L r]$$

$$\left.+\frac{I}{\delta}[(\overline{\alpha_0}+e_0^b r^b)\overline{\alpha_L}e_L r+(\overline{\beta_L}+e_L r)\overline{\alpha_0}e_L^b r^b]+\frac{J^b-J}{\delta}\,\frac{D}{N^b N\delta}\,(\overline{\alpha_0}\overline{\beta_L}e_0 e_L^b-\overline{\alpha_L}\overline{\beta_0}e_L e_0^b)\right\}X_{LS}. \tag{104}$$

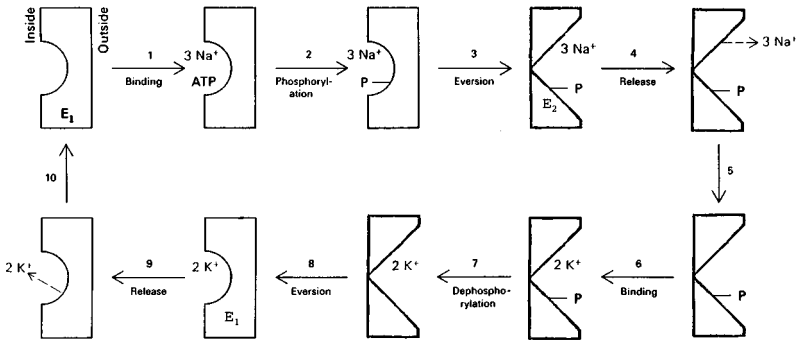


FIG. 4. The sodium-potassium ATPase in state $E_1$ binds sodium from the inside (1), which facilitates the binding of ATP (1) and phosphorylation of an aspartate residue (2). Eversion to enzyme state $E_2$ ensues (3). Here we show the standard model in which the phosphorylation site also everts but to which we raise objections in the text. Sodium is released (4) and potassium is bound [(5) and (6)], both on the outside of the membrane. Dephosphorylation occurs (7) followed by eversion of the potassium binding site (8) and release of potassium to the inside (9). State $E_2$ relaxes to state $E_1$ (10), completing the cycle.

If we solve Eq. (104) for $X_{LS}$ and substitute it into Eqs. (101)–(103), then we obtain explicit solutions for all quantities in terms of the total amount of enzyme in all forms, $E$.

Of particular interest are the fluxes given by the right-hand sides of Eqs. (89) and (90). These determine the nature of the cycling of the enzyme between phosphorylated and dephosphorylated states. Using Eqs. (101)–(103), we find the numerator; $\mathcal{N}$,

$$\mathcal{N}[-r^b(X_{LS}e_L^b - X_{0S}e_0^b)] \propto r r^b(\overline{\alpha_L}\overline{\beta_0}e_L e_0^b - \overline{\alpha_0}\overline{\beta_L}e_0 e_L^b), \tag{105}$$

$$\mathcal{N}[-r(Y_{LS}e_L - Y_{0S}e_0)] \propto -r r^b(\overline{\alpha_L}\overline{\beta_0}e_L e_0^b - \overline{\alpha_0}\overline{\beta_L}e_0 e_L^b). \tag{106}$$

From Eq. (58) and the properties given earlier regarding the conformation potentials, i.e., $V(0)<V(L)$, $V^b(L)<V^b(0)$, and both $V(L)-V(0)$ and $V^b(0)-V^b(L)$ of order several times $k_BT$, it follows that

$$e_L \gg e_0, \quad e_0^b \gg e_L^b. \tag{107}$$

Moreover, even though $\mu_0$ depends on $[Ca^{2+}]^2$ on the inside, at typical phyisiological values around $10^{-7}$ m$M$, the strong affinity of $E_1$ for calcium implies

$$\mu_0 > \nu_0. \tag{108}$$

A similar argument holds for $\beta_L$, which depends on the outside value of $[Ca^{2+}]^2$, which is typically around $10^{-5}$ m$M$. Even though this is a higher calcium concentration than inside, the affinity for calcium of Ca$E_2$-$P$ is relatively weak. Thus, at physiological calcium concentrations we have

$$\alpha_L > \beta_L. \tag{109}$$

These last two inequalities are generally weaker than those in Eq. (107). Since $\alpha_0$ depends on [ADP] and $\beta_0$ depends on [ATP] and aspartate phosphorylation by ATP is energetically uphill at standard state ($+5.7$ kcal/mol), a physiological phosphate state with a ratio (such ratios with apparent dimensions are referred to as molar quantities by convention and are taken as dimensionless) of [ATP] to [ADP] $[P_i]$ of order 500 [5] will provide a favorable direction to the reaction. Under these conditions we may have

$$\beta_0 \approx \alpha_0. \tag{110}$$

Finally, even though $\mu_L$ depends on $[P_i]$, the physiologically low value of $[P_i]$ and the great release in free energy attendant to aspartyl phosphate hydrolysis implies

$$\nu_L \gg \mu_L. \tag{111}$$

Putting inequalities (107)–(111) together with Eq. (100) yields

$$\frac{\overline{\alpha_L}\overline{\beta_0}e_L e_0^b}{\overline{\alpha_0}\overline{\beta_L}e_0 e_L^b} = \frac{\nu_L \mu_0 e_L e_0^b}{\nu_0 \mu_L e_0 e_L^b} \gg 1. \tag{112}$$

Thus the flux in Eq. (105) is strongly positive and that in Eq. (106) is strongly negative. This means there is a robust cycling of enzyme between the two states that results in a net transport of calcium against a calcium gradient. If the physiologically high [ATP]/[ADP][$P_i$] ratio is allowed to degenerate, then these fluxes will fall until they vanish. Clearly, metabolic free energy is being utilized to drive this process. Nevertheless, it has been used to bias the boundary conditions for two diffusions, one for phosphorylated enzyme and one for dephosphorylated enzyme. The energy for the conformation changes represented by these diffusions is the thermal energy of Brownian movement in the diffusion limit.

Another biologically important $P$-type ATPase is the sodium-potassium ATPase that mediates the counterexchange of three $Na^+$ ions for two $K^+$ ions (see Fig. 4). The sodium ions go from inside to outside and the potassium ions do the reverse. Such an ''antiporter'' mechanism is responsible for the resting potential of neurons.

The mechanism for this ATPase has striking similarities to that of the calcium ATPase just analyzed. Binding of three $Na^+$ ions to the $E_1$ state of the enzyme facilitates the binding of ATP and the subsequent phosphorylation of a particular aspartate residue, yielding Na$E_1$-$P$. This is followed by a conformation change that results in the eversion of the sodium binding site, yielding Na$E_2$-$P$. This conformation has a weaker affinity for sodium that is released to the outside.

So far, these steps precisely parallel the initial steps in the calcium ATPase mechanism given by Eqs. (77)–(80). Now something different happens. Before dephosphorylation occurs, two $K^+$ ions bind instead, yielding $KE_2$-$P$. This state dephosphorylates and then everts, releasing the potassium to the inside. That is, $KE_2$-$P$ becomes $KE_2$, which conformationally relaxes to $KE_1$, which releases potassium becoming $E_1$ all over again. This means that the analogs to Eqs. (81) and (82) are instead four steps:

$$E_2 - P + 2K^+ \leftrightarrow KE_2 - P, \tag{113}$$

$$KE_2 - P \leftrightarrow KE_2 + P_i, \tag{114}$$

$$KE_2 \leftrightarrow KE_1, \tag{115}$$

$$KE_1 \leftrightarrow E_1 + 2K^+. \tag{116}$$

Equations (113), (114), and (116) are mass action reactions, whereas Eq. (115) is the conformation relaxation, the analog of Eq. (82), and is modeled as a diffusion process like that given by Eq. (47). Without presenting all of the details, it should be clear that the outcome will be parallel to that for the calcium ATPase, with the simple difference that here the inward flux [cf. Eq. (90)] carries potassium inward as well as changing the enzyme conformation back to its initial state.

One technical point needs to be added here. In all published treatments of the ($Na^+$-$K^+$) ATPase mechanism that we have seen [4,5,19,21,22], diagrams are presented that show the aspartyl phosphate closely associated with the sodium and potassium binding sites so that dephosphorylation is depicted as occurring on the outside of the membrane (see Fig. 4). This amounts to a transport of phosphate in addition to the antiporting of sodium and potassium. Since phosphate carries a double negative charge at *p*H 7, this would seriously affect the overall energetics. We have not found any experimental evidence for such concomitant phosphate transport in this system and strongly suspect that the situation is really parallel with that for the calcium ATPase mechanism described above, i.e., phosphate acts allosterically and remains on the inside surface of the membrane throughout the ion binding site eversion cycle. Even the story for calcium ATPase is confused in the textbooks, with one [5] having phosphate remain on the inside, as we have modeled it here, and another [19] having it transported across the membrane. In our view, the close coupling of the aspartyl phosphate hydrolysis with the potassium transport in the ($Na^+$-$K^+$) ATPase case is an artifact of the perspective in which the free energy released is somehow directly coupled to energizing the ion transport. Since our perspective is that of rectified Brownian movement, the energy of ion transport is purely thermal and the free energy of phosphate hydrolysis merely affects the boundary conditions for the associated conformation state diffusion processes. Thus one very clear conclusion of the rectified Brownian movement perspective for ATPase ion transporters is that aspartyl phosphorylation and dephosphorylation is an allosteric control with the aspartate residue always on the same side of the membrane, the inside in the two cases discussed here. This will keep the phosphate on the inside, a clearly testable hypothesis.

## V. ROTARY ENZYME COMPLEXES

Three classes of rotary enzyme complexes will be discussed here. Each involves one of the three prosthetic groups: lipoamide, biocytin, or phosphopantetheine (see Fig. 5). Several instances of the occurrence of each exist in metabolism [5,19].

Lipoamide is a component of a large multisubunit enzyme complex both for pyruvate dehydrogenase (60 subunits in *E. coli* and 72 subunits in eukaryotic yeast) and for $\alpha$-ketoglutarate dehydrogenase [5,19]. The former occurs in the pathway connecting glycolysis to the citric acid cycle by conversion of pyruvate into acetyl-Co A (coenzyme A). The latter occurs in the citric acid cycle. Both enzyme complexes share many similarities. Indeed, the subunit responsible for reoxidation of lipoamide during its functional cycle is identical in the two complexes. Lipoamide is a 14-Å long flexible attachment arm made from an amide linkage of the carboxyl group of lipoic acid with the $\varepsilon$-amino acid group of lysine, an integral amino acid of the dihydrolipoyl transacetylase subunit of the complex. Two sulfur atoms make up the active head portion of the lipoamide arm. These are separated from the carboxyl group in lipoic acid by a $—(CH_2)_4—$ hydrocarbon stretch that is very flexible since each carbon-carbon bond is a single bond with ease of rotation [5]. Similarly, the amino group of lysine is attached to the $\alpha$ carbon of lysine by an identical $—(CH_2)_4—$ stretch. This makes lipoamide very flexible as an attachment arm for the intermediate acetyl group in the case of pyruvate dehydrogenase (succinyl group in the case of $\alpha$-ketoglutarate dehydrogenase). During the course of the five reactions required for conversion of pyruvate into acetyl-Co*A*, lipoamide is responsible for three. Its oxidized form receives the acetyl group from thiamine pyrophosphate (TPP) and gives it up to reduced coenzyme *A* (Co*A*-SH), becoming reduced itself in the process. To return to its acetyl acceptor state, it must be reoxidized by oxidized flavin adenine dinucleotide (FAD), which gets reduced, to $FADH_2$. These three steps occur at three different sites of the enzyme complex (the complex is highly redundant with 24 lipolyl groups per complex in *E. coli* and 30 in eukaryotes). The flexibility of the lipoamide arm enables it to visit these sites by Brownian movement. Rather than think of the lipoamide arm as a rotating rigid arm of 14 Å length, it is much closer to reality to view the active sulfur containing head as engaging in a tethered random walk. Thus these complexes are effectively rotary without actually being rigid rotors.

Biocytin is a component of enzyme complexes that involve the incorporation of $CO_2$ into organic molecules. It is a $CO_2$ carrier. It is present in the conversion of pyruvate into oxaloacetate, a citric acid cycle intermediate, and it is present in the initial activation steps in fatty acid synthesis when malonyl-Co*A* is formed [5,19]. Biocytin is also a 14-Å-long flexible attachment arm made from an amide linkage of the carboxyl group of biotin with the $\varepsilon$-amino group of lysine, an integral amino acid of the enzyme complex. The active portion of biotin is a heterocyclic ring containing carbon, nitrogen, and sulfur. This time, it is a particular nitrogen atom of the ring that is the site for $CO_2$ attachment that yields carboxyl biotin. Biotin's active head is separated from its carboxyl group by a $—(CH_2)_4—$ hydrocarbon stretch, just as in lipoic acid. Thus biocytin contains two such stretches and is

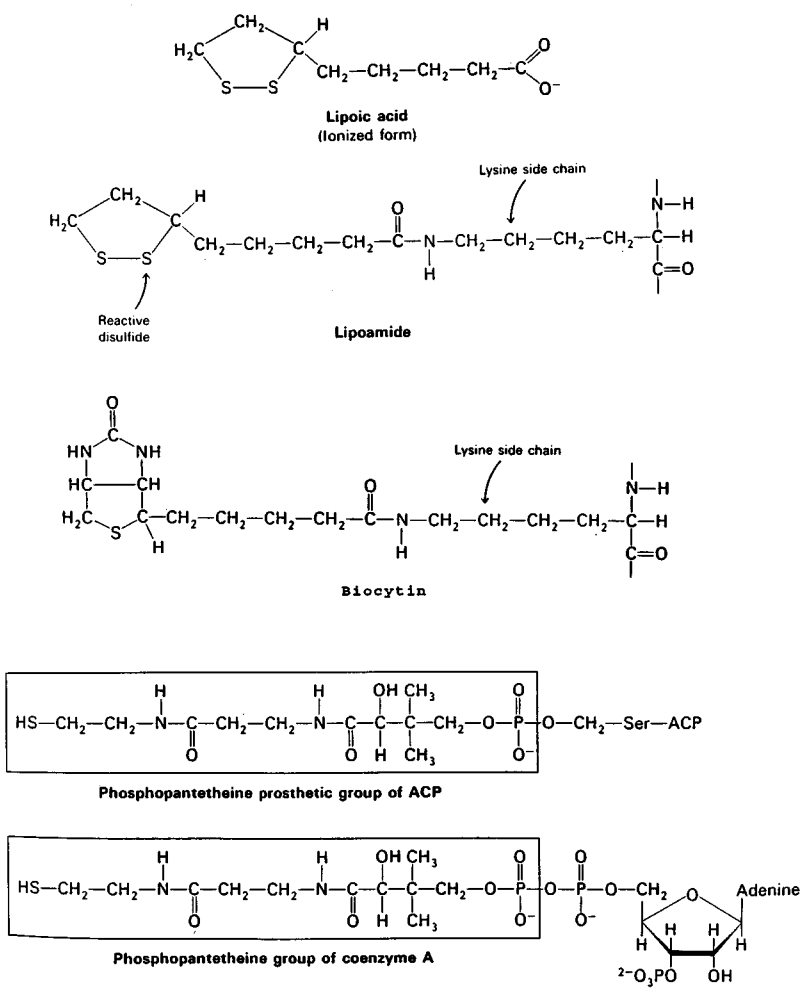


FIG. 5. The structures of lipoic acid, lipoamide, biocytin, and phosphopantetheine attached to acyl carrier protein (ACP) and attached to adenosin monophosphate as coenzyme *A* are shown.

very flexible just like lipoamide. In pyruvate carboxylase, $CO_2$ is attached at one site of the complex and is transferred to pyruvate, forming oxaloacetate, at another site. A tethered Brownian movement or random walk is again the mechanism of this active arm's shuttling between reactive sites of the complex.

Phosphopantetheine is a component of enzyme complexes involved in fatty acid synthesis and in the synthesis of peptide antibiotics such as gramicidin and tyrocidine. It is a 20-Å-long attachment arm with a thiol (—SH) sulfur at one end. It may be thought of structurally as an amide linkage of the amino group of $\beta$-mercaptoethylamine with the carboxyl group of phosphopantothenate, which is itself an amide linkage of two parts. Various acyl groups can form thioesters with the sulfur end, whereas the phosphate end forms a dehydration linkage with the hydroxyl group of serine, an integral amino acid of the acyl carrier enzyme complex [5,19]. Phosphopantetheine can also link up with adenosine monophosphate to form Co*A*-SH. Thus, when attached to serine in the enzyme complex, we may think of this structure as a giant form of Co*A*-SH. Indeed, in fatty acid synthesis, it is the enzyme complex that is required, but in fatty acid degradation only Co*A*-SH is needed. In fatty acid synthesis, nine reaction steps take place per cycle with phosphopantetheine involved in eight. It carries the various intermediates from reactive site to reactive site. Phosphopantetheine contains two stretches of $—(CH_2)_2—$ rather than of $—(CH_2)_4—$ as in lipoamide and biocytin. It also has two amide linkages, as compared to only one for lipoamide and biocytin, and since amides are quite rigid, the net effect is that phosphopantetheine is relatively less flexible than lipoamide and biocytin and is more like a rigid rod. Thus its tethered Brownian movement may be viewed as more like random rotation around the serine attachment site of the complex. This is the evolutionary beginning of a truly rotary enzyme.

Each of these systems may be modeled in a similar fashion. Explicit details are given for biocytin and lipoamide, which are, respectively, two-site and three-site cases. The phosphopantetheine, fatty acid synthetase case, with nine sites will be left to the reader as a straightforward generalization. In general, label the $n$ sites with consecutive integers, $1,2,\ldots,n$. When the enzyme complex arm is at site $i$, it is denoted by $E_i$. We may associate a conformation coordinate with these states just as we did for the $P$-type ATPases. However, here such a coordinate is connected with the true spatial position of the flexible, movable arm of the complex. Although this is really a three-dimensional coordinate, we continue to use the one-dimensional variable $x$ to capture its significance. For example, in the two-site case of biocytin, site 1 would correspond to $x=0$ and site 2 would correspond

to $x=L$, as before. For three sites, as in the case of lipoamide, site 1 would correspond to $x=0$, site 2 to $x=L/2$, and site 3 to $x=L$. This amounts to a nonlinear mapping of three-dimensional space onto a one-dimensional space. If the attachment arm were truly a rigid rod then the natural choice for the one-dimensional parameter would be the rotation angle. Because the attachment arms are flexible, however, their active heads engage in a random walk that is represented by the coordinate $x$. Since motion in this space is Brownian movement and one parameter, the diffusion constant, determines all of its properties, this phenomenological treatment will give only order of magnitude results. Numerical molecular-dynamics simulations of the actual three-dimensional motions of a flexible attachment arm would be required for a more quantitatively realistic treatment.

Let Carb-$P$ denote carboxy phosphate, let $P_i$ denote inorganic phosphate, let Carb-$E_1$ denote carboxy biocytin at site 1, let Carb-$E_2$ denote carboxy biocytin at site 2, let Pyr denote pyruvate, and let Oxa denote oxaloacetate. The biocytin two site system is described by the equations

$$E_1+\text{Carb}-P\underset{\alpha_0}{\overset{\beta_0}{\leftrightarrow}}\text{Carb}-E_1+P_i, \tag{117}$$

$$\text{Carb}-E_1\leftrightarrow\text{Carb}-E_2, \tag{118}$$

$$\text{Carb}-E_2+\text{Pyr}\underset{\beta_L}{\overset{\alpha_L}{\leftrightarrow}}E_2+\text{Oxa}, \tag{119}$$

$$E_2\leftrightarrow E_1. \tag{120}$$

The parallels with Eqs. (42)–(45), (77)–(82), and the ubiquinone dynamics of Eqs. (11), (12), (16), and (17) should be obvious when one thinks of the binding sites here, i.e., the loci of the mass action reactions, as corresponding to the boundary layers in these other cases. Equations (117) and (119) represent mass action reactions, whereas Eqs. (118) and (120) represent diffusion processes in the $x$ coordinate. The concentrations of Carb-$P$, $P_i$, Pyr, and Oxa are maintained fixed by the steady-state metabolism in which these substances participate in many other reactions than in just this single $CO_2$ transfer. In fact, Carb-$P$ is synthesized at site 1 of the biocytin enzyme complex from ATP and bicarbonate ($HCO_3^-$), the dissolved form of $CO_2$. This step releases ADP, which with the $P_i$ released in reaction (117) is converted back into ATP by energy metabolism. The $\alpha$'s and $\beta$'s here are of course different from those in Eqs. (42)–(45), (77)–(82), or the ubiquinone dynamics because of the different chemical species involved. Thus $\alpha_0$ is proportional to $[P_i]$, $\beta_0$ is proportional to [Carb-P], $\alpha_L$ is proportional to [Pyr], and $\beta_L$ is proportional to [Oxa]. Ongoing energy metabolism keeps both [Carb-P] and [Pyr] relatively high and both $[P_i]$ and [Oxa] relatively low. In addition, the standard state Gibbs free-energy change associated with the combination of reactions (117) and (119) is negative. Thus we have the physiological steady-state inequalities

$$\beta_0>\alpha_0, \quad \alpha_L>\beta_L. \tag{121}$$

These inequalities are the same as those given just below Eq. (26). These inequalities create the boundary conditions for the diffusion processes (118) and (120), which amount to rectified Brownian movement, as was seen in each of the earlier discussions. In fact, the parallel with the ubiquinone analysis is even stronger if we do not assume any sort of potential $V(x)$ or $V^b(x)$ acting during the diffusions in Eqs. (118) and (120). The flux results in Eqs. (37) and (38) would apply and would mean here that there would be a nonzero flux from left to right from diffusion (118) and a nonzero flux also from left to right from diffusion (120), both at steady state. In this case, however, it would be natural to use different diffusion constants for the two cases because the heads of biocytin and carboxy biocytin are somewhat different, although not by much (347 d for carboxy biocytin versus 303 d for biocytin).

A special sort of potential, however, is not unreasonable. When $E$ is near site 1, there should be some attraction between the $E_1$ state and the Carb-$P$ binding site. This is a result of complementary weak interactions that produce the selective recognition of the Carb-$P$ bound enzyme site for $E_1$. Similarly, when Carb-$E$ is near site 2, there should be some attraction between the Carb-$E_2$ state and the Pyr bound enzyme. This too is a result of complementary weak interactions. With the former, we associate $V(x)$ and with the latter we associate $V^b(x)$. These potentials are essentially flat, except for a small region near the binding sites. This region is determined by the Debye length, which is of order 8 Å at physiological ionic strength [4], because the weak interactions are essentially electrostatic except at very short range where van der Waals forces and hydrophobic or hydrophilic effects also contribute. This creates an attraction over a distance somewhat larger than the size of the boundary layer associated with the binding site itself. Thus the type of potential-dependent analysis we used for the $P$-type ATPase is more appropriate and again nonzero fluxes of the sort just described are obtained. The net result of this analysis is that the enzyme arm endlessly cycles between the $E_1$ and $E_2$ states in a steady state.

Let HE-TPP denote $\alpha$-hydroxyethyl-TPP, $AE_1$ denote acetyllipoamide at site 1, and $AE_2$ denote acetyllipoamide at site 2. Let $H_2E_2$ denote reduced lipoamide at site 2 and let $H_2E_3$ denote reduced lipoamide at site 3. Finally, let $E_3$ denote oxidized lipoamide at site 3 and $E_1$ denote oxidized lipoamide at site 1. The pyruvate dehydrogenase lipoamide three-site system is described by the equations

$$E_1+\text{HE-TPP}\underset{\alpha_0}{\overset{\beta_0}{\leftrightarrow}}AE_1+\text{TPP}, \tag{122}$$

$$AE_1\leftrightarrow AE_2, \tag{123}$$

$$AE_2+\text{Co}A-\text{SH}\underset{\beta_{L/2}}{\overset{\alpha_{L/2}}{\leftrightarrow}}H_2E_2+\text{acetyl}-\text{Co}A, \tag{124}$$

$$H_2E_2\leftrightarrow H_2E_3, \tag{125}$$

$$H_2E_3+\text{FAD}\underset{\beta_L}{\overset{\alpha_L}{\leftrightarrow}}E_3+\text{FADH}_2, \tag{126}$$

$$E_3\leftrightarrow E_1. \tag{127}$$

We have here three mass action equations (122), (124), and (126) that may be thought of as occurring within boundary layers associated with the binding sites and three diffusion processes (123), (125), and (127). As in the biocytin case, the diffusion constants will be slightly different because the carrier head has groups of different masses on it between the different pairs of sites. Moreover, the $\alpha$'s and $\beta$'s are proportional to their respective cofactors: TPP, HE-TPP, Co*A*-SH, acetyl-Co*A*, FAD, and $FADH_2$. Three of these, HE-TPP, Co*A*-SH, and FAD, are regenerated by active energy metabolism and another three TPP, acetyl-Co*A*, and $FADH_2$, are consumed by active energy metabolism. HE-TPP in particular is produced from pyruvate, the end product of active glycolysis. In addition, the standard state Gibbs free-energy change associated with the combination of reactions (122), (124), and (126) is negative. These facts produce inequalities analogous to Eq. (121),

$$\beta_0 > \alpha_0, \quad \alpha_{L/2} > \beta_{L/2}, \quad \alpha_L > \beta_L . \tag{128}$$

Once again, these inequalities create the boundary conditions for the diffusions that amount to rectified Brownian movement. The result is nonzero fluxes from left to right in each of Eqs. (123), (125), and (127). Thus, in a steady state, the average behavior is a sustained cycling through sites 1, 2, and 3 as if the lipoamide attachment arm were rotating around its lysine connection to the enzyme complex, i.e., like a rotary motor.

We may also invoke the Langevin equivalents of the diffusion processes, as was discussed earlier, and reinterpret this process for a single lipoamide arm. In this interpretation, the arm undergoes Brownian movement from site to site with net flux appearing only as an averaged consequence. For example, when $AE$ arrives at site 3 where FAD is bound, two additional stochastic events occur. First there is some chance that $AE_3$ will actually bind the enzyme, which is governed by the particular potential $V^b(x)$ appropriate for site 3, and second there is some chance that the reaction (126) will actually take place, which is governed by the rate constants $\alpha_L$ and $\beta_L$. We have invoked potentials such as were discussed for the biocytin case. These provide the selective binding of the different modified lipoamides to the different sites.

We emphasize that in both cases, the motion of the attachment arm is entirely the result of thermal agitation, i.e., Brownian movement, and that metabolic energy has been used to bias the boundary conditions by providing reactants on one side of the diffusion and taking away products on the other. For a two-site system, this results in an apparent switching back and forth between sites, whereas in a three- or greater-site system, it results in apparent rotary action. We say ''apparent'' because it is only the statistically averaged behavior that is a simple rotary motion, while the actual motion for any single molecular arm is randomly rotating both clockwise and counterclockwise with a net bias in one of the two directions.

At any particular site, the standard state Gibbs free-energy change of the reactive species may be negative or reactants are supplied by metabolism while products are consumed by metabolism, or both. If the standard state Gibbs free-energy change is not negative, then the production of reactants and the consumption of products by metabolism must be sufficient to overcome the positive standard state Gibbs free-energy change in order to achieve the inequalities (128). For example, the Gibbs free-energy change for reaction (117) is

$$\Delta G = \Delta G^{0\prime} + RT \ln\left(\frac{[\mathrm{Carb}-E_1][P_i]}{[E_1][\mathrm{Carb}-P]}\right). \tag{129}$$

It is the combination of both terms on the right-hand side of this equation that must make $\Delta G < 0$.

## VI. MUSCLE FIBER DYNAMICS

Muscle fibers in skeletal muscle are long bundles of myofibrils [4,5,11,19,23]. Each myofibril is a cylinder shaped, hexagonal array of myofilaments. In the blowfly flight muscle [23], there may be about 700 myofilaments per myofibril with a myofibril cylinder diameter of about 1.5 $\mu$m. When viewed from the side, the myofibrils show a striated pattern that repeats every 2.5 $\mu$m in relaxed muscle, more or less. The ends of these repeating segments are called the $Z$ lines (actually disks viewed on edge) and are produced by transverse meshworks of $\alpha$-actinin, desmin, and vimentin proteins [11,19]. Many long fibrous protein strands of actin, the most abundant protein in many animal cells, are longitudinally attached to these meshworks. These actin molecules are the so-called thin filaments and are typically about 1.0 $\mu$m long with a diameter of 7 nm and are complexes of many identical globular actin protein subunits [5,11]. They are attached to the $Z$ line meshwork in both longitudinal directions with a cross-sectional rectangular array [11]. Interspersed among the actin filaments are the so-called thick filaments made of myosin. Myosin is a protein complex (typically of several hundred single myosin molecules, each of which is itself a complex of six polypeptide chains) typically about 1.5 $\mu$m in length (there are cases where the length is over 5.0 $\mu$m, for which the corresponding $Z$ line spacing is correspondingly longer) with a core diameter of about 15 nm. A central stretch of length 0.3 $\mu$m is devoid of cross-bridges, but both ends possess cross-bridges helically arrayed, as pairs of cross-bridges 180° apart, around the myosin complex core with a longitudinal spacing of 14.3 nm and a relative rotation around the myosin complex axis by 120°. The cross-bridges contain an $S_2$ domain and a pair of $S_1$ domains. One end of the $S_2$ domain is attached to the main complex core by a ''hinge,'' allowing freely articulated motion, and the $S_1$ domains are attached to the other end of the $S_2$ domains by freely articulating hinges (sometimes called ''swivels'') as well [24]. The myosins are attached to the actins by these cross-bridges, with the contact being made with the actin by a binding site of the $S_1$ domain. Together the myosins and actins form a regular, hexagonal array with each myosin surrounded by six actins and each actin surrounded by three myosins. Thus, near the $Z$ lines, the arrangement of the actins changes from hexagonal to rectangular [11]. One segment of myofilaments between two adjacent $Z$ lines is the fundamental unit of muscle tissue and is called a sarcomere [5,11,23]. (Reference [19] has especially nice illustrations of all the muscle fiber features.)

If we view a horizontally lying sarcomere from the side, actin filaments extend to the right from the left $Z$ line and

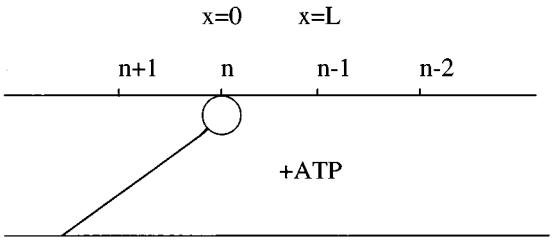


FIG. 6. The upper line denotes a segment of an actin filament featuring the $n$th binding site left of a $Z$ line attachment. The lower line with the articulated arm is a myosin cross-bridge in the rigor state $AM_1$. An ATP molecule is shown waiting to bind the globular myosin head attached to the actin filament.

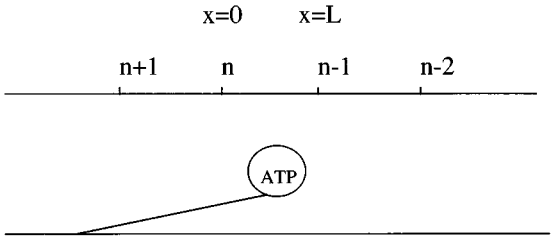


FIG. 7. The ATP-$M_1$ state of myosin is shown detached from the actin.

actin filaments extend to the left from the right $Z$ line. The myosin filaments are symmetrically located midway between the two $Z$ lines such that their ends do not touch the $Z$ lines (the $Z$ line spacing is 2.5 $\mu$m and the myosin complex is only 1.5 $\mu$m long) and such that the ends of the actin filaments do not touch each other (the actins are each only 1.0 $\mu$m long). Thus the only connections holding the two $Z$ lines together are those made by the cross-bridges between myosin filaments and actin filaments (the recently discovered protein titin [19], the largest polypeptide known, connects the myosin complexes elastically to the $Z$ lines, but so far only appears to center the myosin relative to the $Z$ lines and does not facilitate contraction otherwise). Actin fibers are polar and myosins are bipolar. This means that the two ends of the myosins point in opposite directions as do the two sets of actin filaments emanating from the left and right $Z$ lines, respectively. The presently accepted theory for muscle action is that these thin and thick filaments retain their individual lengths at all times, but that by virtue of cross-bridge detachment and reattachment they move past each other, contracting the $Z$ line spacing during exertion (to even somewhat less than 2.0 $\mu$m) and dilating the $Z$ line spacing during relaxation. Generally, the muscle tissue is macroscopically under some tension against which contraction must work, but which is also responsible for the dilation that occurs when muscle is in the relaxed state. This is the ''sliding filament'' model. ''Sliding'' is a bad adjective for contraction since the myosin $S_1$ heads must actively ''walk'' along the actins, but during dilation, sliding seems rather apt. The energy required for the contraction phase is supplied by ATP, which is consumed in vast quantities. ATP binding and hydrolysis occurs on the $S_1$ domains, which therefore contain both the ATPase activity and the actin binding site [5,11,19,25]. One kilowatt of mechanical power per kilogram of dry weight can be switched on in a few milliseconds [11]. The nature of this putative chemomechanical conversion is the focus of our interest in this section.

The fundamental question is, Is there direct chemomechanical conversion of ATP free energy into the work done by muscle or are we once again dealing with rectified Brownian movement [4,5,9,21]? Many accounts of this process clearly invoke a direct chemomechanical conversion mechanism by regarding the ADP and $P_i$ bound state of myosin as ''high energy'' [19] or by referring to the ADP releasing step as the ''power stroke'' [5,11,19]. The power stroke is defined as the set of transitions of the complex of actin, myosin, and phosphates (ATP, ADP, and $P_i$) ''in which chemical energy is transformed into work'' [24]. Others [8,9] clearly favor the rectified Brownian movement mechanism. In the following, we attempt to clearly differentiate these competing views.

One complete cycle of myosin detachment from actin and reattachment to actin involves seven distinct steps (this number is a bit arbitrary since each of these steps involves a set of conformation states). We begin with the state known as ''rigor.'' In the absence of ATP, myosin binds tightly to actin at specific sites on the globular actin subunits, which are spaced about every 5.5 nm [11]. We denote this state by $AM_1$ (Fig. 6). The binding between myosin and actin is apparently between several myosin $S_1$ lysine residues (positive amino groups) and several actin aspartate and glutamate residues (negative carboxyl groups), bolstered by patches of stereospecific hydrophobic amino acid residues of both actin and myosin [19]. $S_1$ also has an ATP binding site to which ATP binds with an attendant detachment of the myosin $S_1$ head from the actin binding site (Fig. 7). This state is denoted by ATP-$M_1$. The ATP is actually bound to a deep cleft in the myosin $S_1$ head [25], opposite but connected to the actin binding site. The binding of ATP allosterically induces destabilization of the myosin $S_1$ head actin binding site, which detaches. Hydrolysis of bound ATP yields an $S_1$ head with bound ADP and bound $P_i$ (since ATP hydrolysis is really $ATP^{4-}+H_2O \rightarrow ADP^{3-}+P_i^{2-}+H^+$, this step immediately releases a proton, $H^+$). This state is denoted by ADP-$M_1$-$P_i$ (Fig. 8). This change in the bound phosphates (ADP and $P_i$ instead of ATP) leads to a readjustment of conformation in the $S_1$ head. By a conformation state diffusion process (Brownian movement) of the type discussed in the ATPase ion transport section, a state denoted by ADP-$M_2$-$P_i$ is visited by the fluctuating $S_1$ head (Fig. 9). This state has a weak binding affinity for an actin binding site, but not for the site from which release was stimulated by ATP binding. Instead, this weak affinity is for the next

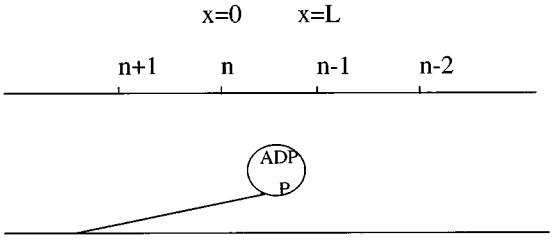


FIG. 8. ATP hydrolysis produces the ADP-$M_1$-$P_i$ state.

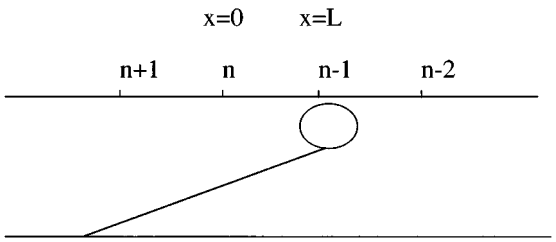


FIG. 9. Conformational relaxation produces the ADP-$M_2$-$P_i$ state. We have suppressed explicit illustration of ADP and $P_i$.

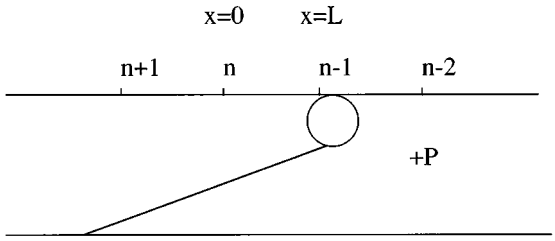


FIG. 11. Release of $P_i$ strengthens the binding and produces the ADP-$AM_2$ state.

actin binding site of the actin fiber (actually some disagreement exists as to whether it is the very next site or whether it skips a site, resulting in a step size of either 5.5 or 11 nm, respectively [9,24]). If we denote the original binding site as site $n$, where $n$ counts how many sites away from the $Z$ line we are, then the reattachment is to either site $n-1$ or site $n-2$. One rationale for this bias is as follows. Reattachment to site $n$ is highly unfavorable because of the binding destabilization caused by the bound phosphates and reattachment to the $n+1$ site is extremely unfavorable because the conformation of the $S_1$ that would potentially permit such binding fails to expose the necessary lysine residues to the complementary aspartate and glutamate residues of the actin binding site. Binding to site $n-1$ (or site $n-2$) is weakly favorable, even though binding to site $n$ has been destabilized because the conformation of state ADP-$M_2$-$P_i$ is compatible with weak binding. Thus the bias in one direction results from the asymmetry of the binding characteristics of the different molecular conformations of the fluctuating $S_1$ head. Another rationale [24] is based on evidence from several sources (e.g., fluorescence and paramagnetic probes, electron micrographs, x-ray diffraction, and sulfhydryl modifications), suggesting that the orientation of the $S_1$ head with respect to the actin binding site remains constant throughout the power stroke and that the repositioning that occurs results from a large-scale change in conformation more distal from the actin instead. In this view, the distal segment perhaps undergoes an $\alpha$-helix, random coil transition. Such a transition permits elongation to position $n-1$ or $n-2$, but it does not permit compression to position $n+1$. The new, weakly bound myosin and actin state is denoted by ADP-$AM_2$-$P_i$ (Fig. 10). Upon release of $P_i$ from the $S_1$ cleft, the binding becomes much stronger, yielding a state we denote by ADP-$AM_2$ (Fig. 11). This is again an allosteric effect. Actin actually stimulates release of $P_i$, and subsequently of ADP, which results in an ATP turnover number of about 10 $s^{-1}$, as opposed to the turnover number of only about 0.05 $s^{-1}$ for isolated myosin [5,19,23]. This activation of ATP turnover number gives actin its name. The allosteric conformation adjustment of the $S_1$ head (or more distal portion) also poises it in a strained conformation, from which it relaxes to a lower-energy state, denoted by ADP-$AM_1$ (Fig. 12). This is all reminiscent of the ATPase ion transporter eversion relaxations discussed earlier. The final step is release of ADP, once again yielding the state $AM_1$ (Fig. 13). The phosphate release steps are rate limiting [24]. Since the myosin is attached to the actin during the relaxation of the conformational strain, there is a relative translation of position of the myosin complex and the actin filament that amounts to a contraction of the sarcomere. This cycle is represented by the system of equations

$$AM_1 + \mathrm{ATP} \underset{\nu_0}{\overset{\rho_0}{\leftrightarrow}} \mathrm{ATP} - M_1 + \mathrm{actin}, \tag{130}$$

$$\mathrm{ATP} - M_1 + \mathrm{H_2O} \underset{\alpha_0}{\overset{\beta_0}{\leftrightarrow}} \mathrm{ADP} - M_1 - P_i, \tag{131}$$

$$\mathrm{ADP} - M_1 - P_i \leftrightarrow \mathrm{ADP} - M_2 - P_i, \tag{132}$$

$$\mathrm{ADP} - M_2 - P_i + \mathrm{actin} \underset{\beta_L}{\overset{\alpha_L}{\leftrightarrow}} \mathrm{ADP} - AM_2 - P_i, \tag{133}$$

$$\mathrm{ADP} - AM_2 - P_i \underset{\mu_L}{\overset{\nu_L}{\leftrightarrow}} \mathrm{ADP} - AM_2 + P_i, \tag{134}$$

$$\mathrm{ADP} - AM_2 \leftrightarrow \mathrm{ADP} - AM_1, \tag{135}$$

$$\mathrm{ADP} - AM_1 \underset{\sigma_0}{\overset{\mu_0}{\leftrightarrow}} AM_1 + \mathrm{ADP}. \tag{136}$$

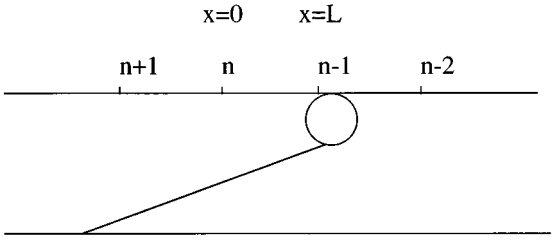


FIG. 10. Tight binding to actin occurs, producing the ADP-$AM_2$-$P_i$ state.

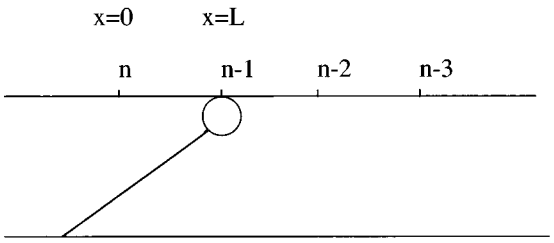


FIG. 12. Conformation relaxation shortens the distance between the myosin cross-bridge attachment site on myosin to the actin binding site. This produces the ADP-$AM_1$ state.

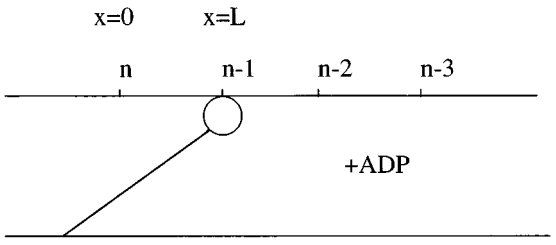


FIG. 13. ADP is released, completing the cycle and regenerating the state $AM_1$ that is depicted in Fig. 6. However, the net effect has been to translate the actin filament to the left relative to the myosin filament.

Steps (132) and (135) are the conformation relaxation steps that we model as diffusions in conformation state space, a manifestation of Brownian movement. The other steps are mass action reactions at specific sites that can be viewed as boundary layers, much as was done in the rotary arm enzyme complex analysis. The concentrations of ATP, ADP, and $P_i$ are maintained fixed by steady-state energy metabolism. This metabolism creates a large $[\mathrm{ATP}]/[\mathrm{ADP}][P_i]$ ratio of roughly $10^5$ [23,26], much larger than was discussed in Sec. IV for the general metabolic level (in muscle, $[\mathrm{ATP}] \sim 10^{-3}$, $[\mathrm{ADP}] \sim 10^{-5}$, and $[P_i] \sim 10^{-3}$).

The conformation relaxation modeled in Eqs. (130)–(132) is a key sequence of steps that differentiates the two fundamentally different models of muscle fiber dynamics. In the chemomechanical conversion models, it is said that the hydrolysis of the ATP bound to myosin ''cocks the $S_1$ head'' [19] or ''resets it for the next interaction'' [5]. In the rectified Brownian movement model presented here, ATP binding and hydrolysis do two things. First, binding of ATP allosterically promotes detachment of myosin from actin, and second, hydrolysis of ATP renders the first act potentially irreversible. The shifting of $S_1$ conformation is solely the result of thermal fluctuations and in no way utilizes the free energy of the ATP. Reaction (134) is another important step. Two effects result. The myosin binding to actin strengthens. This is an allosteric effect of the release of $P_i$. This step is nearly irreversible because of the release of $P_i$. While it is not known yet how the $P_i$ is bound to the myosin cleft, our earlier experience with ATPase ion transport systems suggests that it is covalently bound. If it is bound as a carboxyl phosphate ester such as an aspartyl phosphate, then the hydrolysis step (131) is reversible, but the eventual $P_i$ release is a hydrolysis attended by a big decrease in Gibbs free energy, which would indeed make step (134) highly irreversible. We strongly suspect that this is the case, although we have found no evidence for it to date. Finally, the conformation relaxation modeled in Eq. (135) is the other key step that differentiates the two fundamentally different models of muscle fiber dynamics. This step is often referred to as the power stroke by those implicitly favoring the chemomechanical conversion model [5,19,24]. Because hydrolysis of ATP has occurred some steps earlier, the energy for this power stroke is said to be the energy that was conserved by step (132) when the ATP hydrolysis energy was used to cock the $S_1$ head, which in step (135) finally releases this energy by shifting conformation, i.e., by ''uncocking.'' It has been said [19], ''this complex is a 'high-energy' intermediate in which the free energy of ATP hydrolysis has somehow been conserved.'' As evidence for this view, the fact that ADP-$M$-$P_i$ cannot be formed by simply mixing myosin, ADP, and $P_i$ has been invoked. We believe that this is evidence supporting the fact that myosin in the $AM_1$ state binds ATP, which subsequently hydrolyzes and induces a conformation change in the myosin $S_1$ head, resulting in ADP-$M$-$P_i$. Free myosin $S_1$ heads are in the wrong conformation for direct binding of ADP and $P_i$. Moreover, the decrease in Gibbs free energy attending the release of $P_i$ in the previous step is inconsistent with an additional decrease in Gibbs free energy during step (135). In the former case, an asymmetric boundary condition for Brownian movement is created, whereas, in the latter case, ATP free energy is directly converted into mechanical work. This is a clear differentiation of the two points of view.

The explicit differential equations that follow from Eqs. (130)–(136) parallel those given in Sec. IV by Eqs. (77)–(99) for calcium ATPases if we identify $Z_0$ with ATP-$M_1$, $X_0$ with ADP-$M_1$-$P_i$, $X_L$ with ADP-$M_2$-$P_i$, $Z_L$ with ADP-$AM_2$-$P_i$, $Y_L$ with ADP-$AM_2$, and $Y_0$ with ADP-$AM_1$. We will use $AM_1$ to denote the amount of the tightly bound myosin on actin, also denoted above as $AM_1$. The mass action equations are

$$\frac{d}{dt} Z_0 = \rho_0 AM_1 - \nu_0 Z_0 - \beta_0 Z_0 + \alpha_0 X_0, \tag{137}$$

$$\frac{d}{dt} X_0 = -\alpha_0 X_0 + \beta_0 Z_0 + D \frac{\partial}{\partial x} f(0,t) + \frac{1}{\lambda}\left[\frac{d}{dx} V^b(0)\right] f(0,t), \tag{138}$$

$$\frac{d}{dt} X_L = -\alpha_L X_L + \beta_L Z_L - D \frac{\partial}{\partial x} f(L,t) - \frac{1}{\lambda}\left[\frac{d}{dx} V^b(L)\right] f(L,t), \tag{139}$$

$$\frac{d}{dt} Z_L = \mu_L Y_L - \nu_L Z_L - \beta_L Z_L + \alpha_L X_L, \tag{140}$$

$$\frac{d}{dt} Y_L = -\mu_L Y_L + \nu_L Z_L - D \frac{\partial}{\partial x} g(L,t) - \frac{1}{\lambda}\left[\frac{d}{dx} V(L)\right] g(L,t), \tag{141}$$

$$\frac{d}{dt} Y_0 = -\mu_0 Y_0 + \sigma_0 AM_1 + D \frac{\partial}{\partial x} g(0,t) + \frac{1}{\lambda}\left[\frac{d}{dx} V(0)\right] g(0,t), \tag{142}$$

$$\frac{d}{dt} R_1 = -\rho_0 AM_1 + \nu_0 Z_0 + \mu_0 Y_0 - \sigma_0 AM_1. \tag{143}$$

Equations (137)–(142) parallel Eqs. (83)–(88) and Eq. (143) has no parallel in the earlier case. The potentials $V^b$ and $V$ refer to the $P_i$ bound state of the myosin $S_1$ head and the $P_i$ free, actin attached state of the $S_1$ head, respectively. The conformation coordinate $x$ in this case is directly associated with the position of the myosin $S_1$ head along the actin fiber with $x=0$ referring to the site $n$ position and $x=L$ referring to the site $n-1$ (or $n-2$) position. Thus $V^b(L)<V^b(0)$ reflects the attraction for the new, actin binding site by the ADP-$M_2$-$P_i$ state of the $S_1$ head compared with the lack of attraction of the ADP-$M_1$-$P_i$ state for the original, actin binding site. Similarly, $V(0)<V(L)$ reflects the relaxation of strain in the myosin $S_1$ attachment to the new, actin binding site and the induced relative repositioning of the myosin and actin fibers. In addition to these mass action equations, there are two diffusion equations given by the parallels to Eqs. (47) and (49) wherein $g(x,t)$ now refers to the concentration of ADP-$AM$ and $f(x,t)$ refers to the concentration of ADP-$M$-$P_i$. We may think of the sites of the mass action equations as the boundary layers for these two diffusion processes. As in the ubiquinone analysis, these diffusions are the result of very low Reynolds number Brownian movement in which the inertial terms may be neglected. The rate constants in Eqs. (137)–(143) are different from those for the calcium ATPases that they parallel. Here $\rho_0$ is proportional to [ATP], $\beta_0$ is proportional to $[H_2O]$, $\alpha_L$ is proportional to the activity of actin, $\mu_L$ is proportional to $[P_i]$, and $\sigma_0$ is proportional to [ADP]. These concentrations are maintained at steady-state values by active metabolism (see above).

The steady-state solutions to Eqs. (137), (140), and (143), after some algebra, are

$$AM_{1S}=\frac{\nu_0 Z_{0S}+\mu_0 Y_{0S}}{\rho_0+\sigma_0}, \tag{144}$$

$$Z_{LS}=\frac{\mu_L Y_{LS}+\alpha_L X_{LS}}{\nu_L+\beta_L}, \tag{145}$$

$$Z_{0S}=\frac{\alpha_0(\rho_0+\sigma_0)}{(\nu_0+\beta_0)\sigma_0+\rho_0\beta_0}X_{0S}+\frac{\rho_0\mu_0}{(\nu_0+\beta_0)\sigma_0+\rho_0\beta_0}Y_{0S}. \tag{146}$$

The steady-state fluxes for Eqs. (138), (139), (141) and (142) are deduced from Eqs. (47), (49)–(51), (89), and (90). When these are substituted, we obtain the parallels to Eqs. (63)–(66), (91), (92), (94), and (95). These are

$$-\alpha_0 X_{0S}+\beta_0 Z_{0S}+r^b(X_{LS}e_L^b-X_{0S}e_0^b)=0, \tag{147}$$

$$-\mu_0 Y_{0S}+\sigma_0 AM_{1s}+r(Y_{LS}e_L-Y_{0S}e_0)=0, \tag{148}$$

$$-\alpha_L X_{LS}+\beta_L Z_{LS}-r^b(X_{LS}e_L^b-X_{0S}e_0^b)=0, \tag{149}$$

$$-\mu_L Y_{LS}+\nu_L Z_{LS}-r(Y_{LS}e_L-Y_{0S}e_0)=0. \tag{150}$$

Conservation equations (67) and (97) must also be modified for the present case. Here we need the total myosin conservation equation that parallels Eqs. (57), (67), and (97) and is

$$AM_{1S}+X_{0S}+Y_{0S}+Z_{0S}+X_{0S}\frac{I^b}{\delta}+\frac{J^b}{N^b\delta}(X_{LS}e_L^b-X_{0S}e_0^b)$$

$$+X_{LS}+Y_{LS}+Z_{LS}+Y_{0S}\frac{I}{\delta}+\frac{J}{N\delta}(Y_{LS}e_L-Y_{0S}e_0)=M, \tag{151}$$

where $M$ denotes the total amount of myosin in all possible states: $AM_1$, ATP-$M_1$, ADP-$M_1$-$P_i$, ADP-$M_x$-$P_i$, ADP-$M_2$-$P_i$, ADP-$AM_2$-$P_i$, ADP-$AM_2$, ADP-$AM_x$, and ADP-$AM_1$. The two expressions ADP-$M_x$-$P_i$ and ADP-$AM_x$ refer to the quantities represented by the densities $f(x)$ and $g(x)$, respectively. By substituting Eqs. (144)–(146) into Eqs. (147)–(150), we obtain precisely Eqs. (91), (92), (94), and (95) if $\mu_0$ and $\nu_0$ of Eq. (92) are replaced by $\overline{\mu_0}$ and $\overline{\nu_0}$ defined by

$$\overline{\mu_0}=\frac{\rho_0\mu_0}{\rho_0+\sigma_0}, \qquad \overline{\nu_0}=\frac{\sigma_0\nu_0}{\rho_0+\sigma_0}. \tag{152}$$

This means that the steady-state solutions given by Eqs. (101)–(103) work here also, provided in the definitions of Eq. (100), $\mu_0$ and $\nu_0$ are replaced by $\overline{\mu_0}$ and $\overline{\nu_0}$. With these changes, the flux numerators in Eqs. (105) and (106) are still applicable. Only Eq. (104) becomes significantly more complicated because of the relatively complicated change from Eq. (98) to Eq. (146) and because of the presence of $AM_{1S}$ in Eq. (151). Nevertheless, after an algebraic excursion, we find

$$AM_{1S}+Z_{0S}=\frac{\alpha_0(\rho_0+\nu_0+\sigma_0)}{(\beta_0+\nu_0)\sigma_0+\rho_0\beta_0}X_{0S}$$

$$+\frac{\mu_0(\rho_0+\nu_0+\beta_0)}{(\beta_0+\nu_0)\sigma_0+\rho_0\beta_0}Y_{0S}. \tag{153}$$

This enables us to convert Eq. (151) into the parallel of Eq. (104), which is

$$M=[(\overline{\alpha_0}e_0r+\overline{\beta_0}e_0^br^b)\overline{\beta_L}+(\overline{\beta_0}e_L+\overline{\beta_L}e_0)e_0^brr^b]^{-1}\Bigg\{\left(1+\frac{\alpha_L}{\beta_L+\nu_L}\right)[(\overline{\alpha_0}e_0r+\overline{\beta_0}e_0^br^b)\overline{\beta_L}+(\overline{\beta_0}e_L+\overline{\beta_L}e_0)e_0^brr^b]$$
$$+\left(1+\frac{\alpha_0(\rho_0+\nu_0+\sigma_0)}{(\beta_0+\nu_0)\sigma_0+\rho_0\beta_0}\right)[(\overline{\beta_0}+e_0r)\overline{\beta_L}e_L^br^b+(\overline{\alpha_L}+e_L^br^b)\overline{\beta_0}e_Lr]+\left(1+\frac{\mu_0(\rho_0+\nu_0+\beta_0)}{(\beta_0+\nu_0)\sigma_0+\rho_0\beta_0}\right)$$
$$\times[(\overline{\alpha_L}e_Lr+\overline{\beta_L}e_L^br^b)\overline{\alpha_0}+(\overline{\alpha_0}e_L^b+\overline{\alpha_L}e_0^b)e_Lrr^b]+\left(1+\frac{\mu_L}{\beta_L+\nu_L}\right)[(\overline{\alpha_0}e_0r+\overline{\beta_0}e_0^br^b)\overline{\alpha_L}+(\overline{\alpha_0}e_L^b+\overline{\alpha_L}e_0^b)e_0rr^b]$$
$$+\frac{I^b}{\delta}[(\overline{\beta_0}+e_0r)\overline{\beta_L}e_L^br^b+(\overline{\alpha_L}+e_L^br^b)\overline{\beta_0}e_Lr]+\frac{I}{\delta}[(\overline{\alpha_0}+e_0^br^b)\overline{\alpha_L}e_Lr+(\overline{\beta_L}+e_Lr)\overline{\alpha_0}e_L^br^b]$$
$$+\frac{J^b-J}{\delta}\frac{D}{N^bN\delta}(\overline{\alpha_0}\overline{\beta_L}e_0e_L^b-\overline{\alpha_L}\overline{\beta_0}e_Le_0^b)\Bigg\}X_{LS}. \tag{154}$$

We remind the reader that the $\overline{\alpha'}$s and $\overline{\beta e}$'s here are given by Eq. (100), in which the replacements of $\mu_0$ and $\nu_0$ by the $\overline{\mu_0}$ and $\overline{\nu_0}$ of Eq. (152) have been made. As before, this equation must be solved for $X_{LS}$ in terms of $M$ and then substituted into Eqs. (101)–(103) to obtain all quantities in terms of $M$.

Definitive kinetic studies for the reactions in Eqs. (130)–(136) are difficult to do. Cooke [24] has reviewed the situation and his conclusions lead us to the following values for the rate constants appearing in Eqs. (130)–(136). In Eq. (130), we have combined ATP binding with the myosin detachment step because ATP binding is very rapid and dissociation is rate limiting. The combined process is quite irreversible because of the ATP binding even though the dissociation segment is nearly reversible, leading to $\rho_0 > \nu_0$ with $\rho_0 \sim 500\ \mathrm{s}^{-1}$. The hydrolysis in Eq. (131) is both slow and nearly reversible, with an equilibrium constant $K_{\mathrm{eq}}$ around 1–10. Thus $\beta_0 \sim \alpha_0$ and $\beta_0 \sim 50\ \mathrm{s}^{-1}$. The actin reattachment step of Eq. (134) is kinetically similar to the reversible dissociation segment of Eq. (130), yielding $\alpha_L \sim \beta_L$ with $\alpha_L \sim 500\ \mathrm{s}^{-1}$. $P_i$ and ADP release are rate limiting for the entire cycle. They are also quite irreversible steps. Thus we have $\nu_L \gg \mu_L$ and $\mu_0 \gg \sigma_0$ with $\nu_L \sim 1-10\ \mathrm{s}^{-1}$ and $\mu_0 \sim 1-10\ \mathrm{s}^{-1}$. Spectroscopic probes used to study the Brownian movement about the hinges connecting the myosin $S_1$ fragment to the $S_2$ fragment and connecting the $S_2$ fragment to the myosin core yield time scales for these processes of order microseconds. Referring back to the definitions in Sec. III, this means that $r^b$ and $r$ are both of the order of $10^6\ \mathrm{s}^{-1}$. Thus we see four distinct time scales during the detachment-reattachment cycle: order $1-10\ \mathrm{s}^{-1}$ for $P_i$ and ADP release, order $10^2\ \mathrm{s}^{-1}$ for ATP hydrolysis, order $10^3\ \mathrm{s}^{-1}$ for myosin-actin dissociation and binding, and order $10^6\ \mathrm{s}^{-1}$ for the Brownian movement of the swiveling cross-bridges.

In order to deduce a quantitative relationship between $M$ and $X_{LS}$ from Eq. (154), it is also necessary to estimate the potentials $V^b$ and $V$ that are used in the definitions in Eqs. (58)–(62). To do this, we draw on the Cordova-Ermentrout-Oster (CEO) model [9(d)], which invokes a harmonic-oscillator potential as was originally suggested by Huxley [8]. This model is different from our model in an important way. In the Huxley-CEO model, the cross-bridge made by the $S_1$-$S_2$ connection is for a Hooke's law spring. For the step in Eq. (132), it must extend in length, thereby increasing the spring's potential energy, whereas in the step in Eq. (135) it contracts, releasing this potential energy as work. The first step requires a thermal fluctuation that provides the energy of extention in the rectified Brownian movement model (in the chemomechanical conversion model, this energy is supplied by ATP hydrolysis, i.e., ATP ''cocks'' the spring). In our model, the step in Eq. (135) is very similar to the Huxley-CEO model step, but the first step in Eq. (132) is distinctly different. In our model, this step is also a relaxation. It is a relaxation of the ADP-$M_1$-$P_i$ conformation to the ADP-$M_2$-$P_i$ conformation. The allosteric change and reversed stability in the myosin head conformation triggered by ATP binding and hydrolysis creates this posture for relaxation by Brownian movement as opposed to creating potential energy instead. Nevertheless, we will estimate the energies involved in both relaxations as if both $V^b$ and $V$ were Hooke's law springs of the Huxley-CEO variety. For Eq. (135) the spring potential is

$$V(x)=\tfrac{1}{2}kx^2, \tag{155}$$

since the $x=0$ site is attractive, and for Eq. (132) the spring potential is

$$V^b(x)=\tfrac{1}{2}k(L-x)^2, \tag{156}$$

since the $x=L$ site is attractive is this case. Such springs are given [9(d)] a Hooke's constant (elastic modulus) $k$ of $k \sim 0.5\ \mathrm{g/s}^2$. If we assume an extension or contraction of order two binding sites, then the distance involved is about 10 nm. This leads to an energy difference between positions $x=0$ and $L$ in our conformation coordinate notation of $\sim 25 \times 10^{-14}$ ergs, or about $6.25 k_B T$. It follows that

$$\frac{e_0^b}{e_L^b}\approx\exp[6.25]=518, \quad \frac{e_L}{e_0}\approx\exp[6.25]=518, \tag{157}$$

with both denominators of order unity.

We are now in a position to estimate all of the parameters in the algebraic expressions characterizing the contraction cycle. We obtain

$$\rho_0 > \nu_0, \quad \rho_0 \sim 500 \ \text{s}^{-1}, \quad \nu_0 \sim 50 \ \text{s}^{-1},$$

$$\beta_0 \sim \alpha_0, \quad \beta_0 \sim 50 \ \text{s}^{-1}, \quad \alpha_0 \sim 10 \ \text{s}^{-1},$$

$$\alpha_L \sim \beta_L, \quad \alpha_L \sim 500 \ \text{s}^{-1}, \quad b \sim 500 \ \text{s}^{-1},$$

$$\nu_L \gg \mu_L, \quad \nu_L \sim 5 \ \text{s}^{-1}, \quad \mu_L \sim 0.5 \ \text{s}^{-1},$$

$$\mu_0 \gg \sigma_0, \quad \mu_0 \sim 5 \ \text{s}^{-1}, \quad \sigma_0 \sim 0.5 \ \text{s}^{-1},$$

$$r, r^b \sim 10^6 \ \text{s}^{-1},$$

$$\overline{\mu_0} = \frac{\rho_0 \mu_0}{\rho_0 + \sigma_0} \sim \mu_0 \sim 5 \ \text{s}^{-1},$$

$$\overline{\nu_0} = \frac{\sigma_0 \nu_0}{\rho_0 + \sigma_0} \sim \frac{\sigma_0}{\rho_0} \nu_0 = \frac{\nu_0}{1000} = 0.05 \ \text{s}^{-1},$$

$$\overline{\alpha_0} = \frac{\overline{\nu_0}}{\beta_0 + \overline{\nu_0}} \alpha_0 \sim \frac{\overline{\nu_0}}{\beta_0} \alpha_0 = \frac{\alpha_0}{1000} = 0.01 \ \text{s}^{-1}, \quad (158)$$

$$\overline{\beta_0} = \frac{\overline{\mu_0}}{\beta_0 + \overline{\nu_0}} \beta_0 \sim \frac{\overline{\mu_0}}{\beta_0} \beta_0 = \overline{\mu_0} \sim \mu_0 \sim 5 \ \text{s}^{-1},$$

$$\overline{\alpha_L} = \frac{\nu_L}{\beta_L + \nu_L} \alpha_L \sim \frac{\alpha_L}{100} = 5 \ \text{s}^{-1},$$

$$\overline{\beta_L} = \frac{\mu_L}{\beta_L + \nu_L} \beta_L \sim \frac{\mu_L}{\beta_L} \beta_L = \mu_L \sim 0.5 \ \text{s}^{-1}.$$

Using Eqs. (155) and (156) in Eqs. (58)–(62), we obtain the following quantities by numerical integration:

$$N = N^b \sim 270 \ \text{nm}, \quad I = 3.75 \ \text{nm}, \quad I^b = 1900 \ \text{nm},$$
$$J = 16.1 \ \text{nm}^2, \quad J^b = 981 \ \text{nm}^2, \quad \delta \sim 0.5 \ \text{nm}. \quad (159)$$

Using these estimates, we can evaluate each of the contributions to Eq. (154). Notice that there is one denominator factor and seven summands on the right-hand side of Eq. (154). For them we obtain

$$M = [1.25 \times 10^{18}]^{-1} \{2.5 \times 10^{18} + 3 \times 10^{15} + 1.4 \times 10^{18} + 2.5 \times 10^{15} + 9.5 \times 10^{18} + 9.4 \times 10^{18} - 4.5 \times 10^{13}\} X_{LS} = 18.24 X_{LS}. \quad (160)$$

From Eqs. (19)–(90), we have the fluxes associated with the Brownian diffusions. In a steady state, they are equal in magnitude and opposite in direction, as is manifest in Eqs. (105) and (106). The magnitude is given by

$$\mathcal{F} = r r^b \frac{\overline{\alpha_L}\overline{\beta_0} e_L e_0^b - \overline{\alpha_0}\overline{\beta_L} e_0 e_L^b}{(\overline{\alpha_0} e_0 r + \overline{\beta_0} e_0^b r^b)\overline{\beta_L} + (\overline{\beta_0} e_L + \overline{\beta_L} e_0) e_0^b r r^b} X_{LS}. \quad (161)$$

Since the denominator here is the same as in Eq. (154), replacing $X_{LS}$ by $M$ results in a cancellation and we get

$$\mathcal{F} = 1.3 M \ \text{s}^{-1}. \quad (162)$$

Since $M$ denotes the amount of myosin present in the sense of the number of molecules, this result means that the myosin cycle requires slightly less than one second per cycle, a quantity invoked in Ref. [24]. Since we have used kinetic parameters given in Ref. [24], this shows the consistency of our model with that of Ref. [24] even though several details are different. Nevertheless, this value for the myosin cycle time is inconsistent with other models, such as in Ref. [9](d), where the cycle time is given as 37 ms. However, it is difficult to reconcile such faster cycle times with the ATP turnover number of $\sim 10 \ \text{s}^{-1}$ that is obtained for actin activated myosin ATPase activity measured in vitro. How can the cycle time be much less than the ATP turnover time if ATP is an obligatory component of each cycle, as it must be in our rectified Brownian movement model?

Our results once again demonstrate how rectified Brownian movement results in a sustained cycle in a steady state. The analysis shows how metabolic free energy is used to bias boundary conditions for diffusions so that nonzero steady-state fluxes are produced.

This model also yields load-velocity profiles for the actin-myosin dynamics. Two distinct types have been observed [9(d)] depending on the nature of the load attached to the actin fiber. In the isotonic case, the load force is constant; its potential is $-Fx$. In the auxotonic case, the load force is linear, such as for a Hooke's law spring; its potential is $\frac{1}{2}K(D-x)^2 - \frac{1}{2}KD^2$, where $D$ is the length of the full extension of the Hooke spring, a length generally much larger than the step length $L$. Both forces oppose the motion of the actin fiber caused by the action of the myosin attachment-detachment cycle. In the second case, we have subtracted a constant in order that the load potential vanishes at $x=0$.

The presence of a load is incorporated into our model through modification of the potential $V(x)$. Since $V(x)$ governs the relaxation of the ADP-$AM_2$ state to the ADP-$AM_1$ state, we simply add the load potential to this potential. Returning to Eqs. (58)–(62), it becomes clear which parameters are load dependent. For example, $e_0$ remains unchanged, but $e_L$ decreases as a result. In our derivation of Eq. (162) from Eqs. (154), (160), and (161), we observed that the $r$ and $r^b$ terms are largest by far. Of the seven summands in the numerator of Eq. (154), we keep only the first, third, fifth, and sixth and only their $rr^b$ dependence at that, for a very good approximation. Substituting this into Eq. (161) yields

$$\mathcal{F} \cong (\overline{\alpha_L}\overline{\beta_0} e_L e_0^b - \overline{\alpha_0}\overline{\beta_L} e_0 e_L^b) \Big\{ 2(\overline{\beta_0} e_L + \overline{\beta_L} e_0) e_0^b + 1.12(\overline{\alpha_0} e_L^b + \overline{\alpha_L} e_0^b) e_L + \frac{I^b}{\delta}(e_0 \overline{\beta_L} e_L^b + e_L^b \overline{\beta_0} e_L) + \frac{I}{\delta}(e_0^b \overline{\alpha_L} e_L + e_L \overline{\alpha_0} e_L^b) \Big\}^{-1} M, \quad (163)$$

wherein we have used the numerical values of the rate constants given in Eq. (158). Using these same constants, it is seen that in each pair of the four terms in the denominator above, one is always about three orders of magnitude bigger than the other, as is the case for the first term in the numerator compared to the second. In each case, this larger term

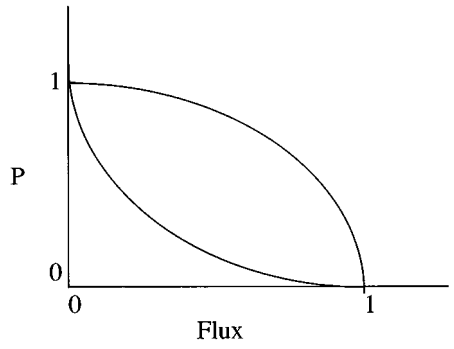


FIG. 14. Isotonic load-velocity profile for $P=F$ and auxotonic load-velocity profile for $P=K$. The flux is the dimensionless scaled flux, which means it has been divided by its value for $P=0$. The $P$ is also scaled by division by the $P$ value that causes the flux to vanish. The lower curve is for $F$ and the upper curve is for $K$. Both are qualitative and exhibit the difference between a positive and a negative second derivative profile.

contains $e_L$, which consequently cancels out of the expression if we only retain these larger terms. Thus we get

$$\mathcal{F}\cong\overline{\alpha_L}\overline{\beta_0}e_0^b\left\{2\overline{\beta_0}e_0^b+1.12\overline{\alpha_L}e_0^b+\frac{I^b}{\delta}e_L^b\overline{\beta_0}+\frac{I}{\delta}e_0^b\overline{\alpha_L}\right\}^{-1}M. \tag{164}$$

Only the parameter $I$ is dependent on the load. This considerably simplifies the remaining analysis, which nevertheless remains rather involved algebraically.

The load-velocity profiles correspond to $F$-$\mathcal{F}$ or $K$-$\mathcal{F}$ profiles for the two cases being considered. What is of interest qualitatively is the shape of the curves. This can be determined by analysis of the first and second derivatives of the flux with respect to $F$ or with respect to $K$. In the Appendix, we show that for the isotonic case, the first derivative of $\mathcal{F}$ with respect to $F$ is negative, while the second derivative is positive. This yields a load-velocity profile such as we got for ubiquinone in Eq. (40). We also show that for the auxotonic case, the first derivative of the flux with respect to $K$ is negative as is the second derivative. This is consistent with other auxotonic models and experiments [9(d)]. These profiles are shown qualitatively in Fig. 14.

## VII. DISCUSSION

In this paper, we have presented support for the idea that many diverse biological processes at the macromolecular and cellular levels of function exhibit rectified Brownian movement. Rectification of the Brownian movement is achieved at the expense of metabolic Gibbs free energy, often supplied by ATP. The actual physical motion, transport of a molecule or ion, rotation of a molecular arm, or the contraction of a sarcomere, is solely the result of thermal energy. This energy is harnessed to do work by asymmetric boundary conditions for the diffusive process driven by thermal energy. These boundary conditions are created at the expense of metabolic energy. We have shown that the paradigmatic model for this mechanism, which is established by a detailed analysis of ubiquinone diffusion in membranes, works in several other contexts as well. Specifically, we have extended the model to include ion transport by $P$-type ATPases, rotary enzyme complexes of three varieties, and even the cross-bridge dynamics of striated muscle. These examples are drawn from an evolutionary continuum of cases suggesting that this fundamental mechanism was established early in evolution and then repeatedly refined for additional purposes.

Several other examples of this basic idea have appeared in the literature. An especially appealing example is the translocation of some proteins through membranes [7,27]. For example, mitochondrial preproteins must cross two membranes to reach the mitochondrial matrix. Specific receptors exist in the membrane for this purpose. The preprotein has a leader sequence of positively charged basic residues. The membrane electrical potential drives the leader through the membrane translocation complex. Then the leader is cleaved. The rest of the process is essentially rectified Brownian movement. The protein could diffuse either way under the influence of thermal fluctuations. However, on the matrix side of the inner membrane, there await a number of proteins, mHsp 70 proteins, that can bind ATP. When they do bind ATP, they allosterically associate with a protein MIM44, which is on the inside of the inner membrane and is associated with the membrane translocation complex, and then they also bind the protein being translocated as it comes through the membrane. This keeps the translocating protein from diffusing backward because the globular mHsp70 complex with the translocating protein is too big to go backward through the membrane translocation complex. The ATP is hydrolyzed, allosterically causing the mHsp70 protein to release its hold on MIM44, thereby allowing it and the translocating protein, to which mHsp70 is still attached, to diffuse inward so that another ATP-bound mHsp70 can attach to MIM44 and to the translocating protein and continue biasing the process. It is said [27] that ''this cycle uses the energy of ATP binding and hydrolysis to drive preprotein movement into the matrix.'' Clearly, it is more precise to say that the ATP cycle simply effectuates a biasing of an otherwise bidirectional Brownian movement so that it is one-way instead. The movement of the preprotein is entirely caused by thermal agitation and not by the energy released upon ATP hydrolysis.

Another beautiful system is the bacterial flagella. This system has recently been analyzed in detail anew [7]. The mechanism, which is quite incredible, involves a flagellar rotor, made of proteins, embedded in the bacterial membrane. This rotor actually rotates and is powered by the transmembrane proton potential that drives protons through stator proteins tightly associated with the rotor [5,10,19]. This recent model involves protons that execute thermally induced jumps between sites on the stator. Electrostatic forces between charges on the stator and on the rotor play a role in the generation of torque. The model is essentially a rectified Brownian movement in the presence of an electrostatic potential. An immediate goal for us is to see if this model can be readily put into the general framework presented in this paper.

To facilitate the analysis of the compatibility of the flagella rotor model with the general setting established in this paper, a simpler rotor system may be easier to analyze first. This simpler system is the $F$-type ATPase [28]. The $F$-type ATPase is responsible for the synthesis of ATP in mitochon-

drial membranes. While complex, it is structurally much simpler than the bacterial flagella system. The Boyer model [29] for its function involves a central protein complex that functions as a rotor. Proton flux through the ATPase drives the rotation of this rotor. The mechanism for this system may prove to be an evolutionary precursor to the flagellar system.

The key question for both rotor models is whether the actual process of rotation is just rotational Brownian movement, whereas the energy released by passage of protons through the membrane is solely for the purpose of biasing the Brownian movement in one direction. In the flagella model [7] it seems that the protons do a bit of both since their positive charge is involved in the electrostatic forces between the stator and the rotor that cause a one-way rotation as well as contributing to the torque. In our general model, we have described how the Brownian movement can involve a potential $V$ or $V^b$. Without expenditure of metabolic energy to bias the Brownian movement in the presence of a potential, nonzero steady-state fluxes will not result. The potentials will merely create nonuniform equilibrium distributions. In these rotor models, the protons may play a dual role by providing both a contribution to the potentials and to the biasing of the boundary conditions. These details require further exploration.

Another fundamental cellular process potentially utilizing rectified Brownian movement is protein translation on ribosomes. In this process, the genetic code transcribed into messenger RNA (mRNA) is translated into amino acid sequences by a process coordinated on ribosomes [5,11,19,23]. This process involves transfer RNAs (tRNA) that both read the codons on the mRNA and carry the cognate amino acids. The process requires that the ribosome systematically progress down the mRNA while amino-acyl tRNAs come into an attachment site on the ribosome, site $A$, take on the growing polypeptide chain from the ribosome $P$ site, and translocate to the adjacent $P$ site so that the next amino-acyl tRNA can come into the $A$ site. These steps involve the utilization of the Gibbs free energy available in the molecular ''cousin'' of ATP, guanosine triphosphate (GTP). Two GTPs are used per amino acid, whereas only one ATP is needed to activate the amino acid for peptide bond synthesis. It is very tempting to suggest that the GTP energy is being used to rectify Brownian movement that then results in the systematic progress of the ribosome along the mRNA. Attachment of an amino-acyl tRNA to the $A$ site of the ribosome requires the elongation factor $EF\text{-}Tu$, which binds and ultimately hydrolyzes GTP. After the peptidyl transfer step, translocation of the peptidyl tRNA from the $A$ site to the $P$ site of the ribosome requires translocation factor EF-G, which also binds and hydrolyzes GTP. These hydrolysis steps appear to render these steps relatively irreversible, thereby biasing the boundary conditions for what would otherwise be a bidirectional Brownian movement of the bound tRNAs. This hypothesis needs to be explored in greater detail.

Similarly, the mechanisms by which DNA polymerase and RNA polymerase read DNA for replication and transcription, respectively, may also be rectified Brownian movement. Thus the behavior of these large enzyme complexes also needs to be investigated from this perspective.

These examples, along with other examples already in the literature, e.g., tubulin dynamics in chromosome movement during mitosis [30], underscore the notion that rectified Brownian movement is functioning at many levels in molecular and cell biology, from enzymes to organelles to the entire mitotic spindle and to muscle. If and when these many examples acquire detailed quantitative analysis consistent with experiments, it will be safe to say that rectified Brownian movement does indeed give life its vitality.

## ACKNOWLEDGMENT

This work was supported by NSF Grant No. PHY-9514853.

## APPENDIX

Let either $F$ or $K$ be denoted by $P$ for the purposes of the analysis in this appendix. Only the parameter $I$ in Eq. (164) depends on $P$. Thus we may express the flux as

$$\mathcal{F} \cong \frac{AM}{B+CI}, \tag{A1}$$

where $A$, $B$, and $C$ are constants, as is the myosin molecule number $M$. The flux derivatives are given by

$$\frac{d\mathcal{F}}{dP} = -\frac{AMC}{(B+CI)^2}\frac{dI}{dP}, \tag{A2}$$

$$\frac{d^2\mathcal{F}}{dP^2} = \frac{AM}{(B+CI)^3}\left[2C^2\left(\frac{dI}{dP}\right)^2 - C(B+CI)\frac{d^2I}{dP^2}\right]. \tag{A3}$$

These expressions reduce the problem to the first and second derivatives of $I$. Equation (60) implies

$$\frac{dI}{dF} = e_0\int_0^L dx\,\frac{x}{k_BT}\exp\left[-\frac{kx^2}{2k_BT}+\frac{Fx}{k_BT}\right] > 0, \tag{A4}$$

$$\frac{dI}{dK} = e_0\int_0^L dx\,\frac{2Dx-x^2}{2k_BT}\exp\left[-\frac{kx^2}{2k_BT}-\frac{K(D-x)^2}{2k_BT}+\frac{KD^2}{2k_BT}\right] > 0. \tag{A5}$$

The first inequality is obvious from the positive integrand, whereas the second follows from the fact that $D \gg L$. Both results imply the negativity of the first flux derivative in Eq. (A2).

Using integration by parts, the integral in Eq. (A4) may be explicitly evaluated and yields

$$\frac{dI}{dF} = \frac{F}{kk_BT}I + \frac{e_0}{k}\left(1-\exp\left[-\frac{kL^2}{2k_BT}+\frac{FL}{k_BT}\right]\right). \tag{A6}$$

We will denote the exponential in this expression by $E(L,F)$ in the following. A similar but longer calculation produces the second derivative in closed form as well

$$\frac{d^2I}{dF^2}=\frac{F}{kk_BT}\left(\frac{F}{kk_BT}\,I+\frac{e_0}{k}\,[1-E(L,F)]\right)+\frac{1}{kk_BT}\,[I-e_0LE(L,F)]. \tag{A7}$$

These results permit us to compute the bracketed expression in Eq. (A3) and we get

$$\begin{aligned}2C^2\left(\frac{dI}{dF}\right)^2-C(B+CI)\,\frac{d^2I}{dF^2}&=CI(CI-B)\left(\frac{F}{kk_BT}\right)^2+(3CI-B)C\,\frac{F}{kk_BT}\,\frac{e_0}{k}\\&\times[1-E(L,F)]+2C^2\left(\frac{e_0}{k}\right)^2[1-E(L,F)]^2\\&+C(CI+B)\,\frac{1}{kk_BT}\,(e_0L-I).\end{aligned} \tag{A8}$$

Since the exponential factors $E(L,F)$ are always less than 1 and since the definition of $I$ in Eq. (60) makes it clear that $I$ is always less than $e_0L$, then the sign of the right-hand side of Eq. (A8) is determined by the signs of $(CI-B)$ and $(3CI-B)$. From Eq. (160), we have that, aside from units that happen to be $s^{-3}$, the magnitude of $B$ is $13.4\times10^{18}$ and that of $CI$ is $9.4\times10^{18}$. This is of course for the $F=0$ case. Since $I$ increases with $F$, this is the worst case. Nevertheless, $3CI-B>0$ and only $CI-B<0$. However, this negative term occurs in Eq. (A8) with a factor of $F^2$, while the positive $3CI-B$ term occurs with a factor of $F$. Even ignoring the other positive terms, this means that the sum is positive for all $F<1.97$ pN as is easily obtained by simple algebra. We also find that as $F$ increases, $I$ increases in accord with Eqs. (A6) and (A7), both of which are positive. A Taylor series shows that $I(F)$ will make $CI-B$ positive for $F>1.0$ pN. Consequently, the right-hand side of Eq. (A8) is always positive and this makes the second flux derivative of Eq. (A3) positive as well. This explains the lower curve of Fig. 14 for the isotonic load case.

Analysis of the auxotonic case is just as straightforward, but involves considerably more algebra. The integral in Eq. (A5) is computed by integration by parts to yield

$$\begin{aligned}\frac{dI}{dK}&=\frac{D}{k_BT}\left[\frac{KD}{K+k}\,I+\frac{k_BT}{K+k}\,e_0[1-E(L,K)]\right]\\&-\frac{1}{2k_BT}\left[\frac{KD}{K+k}\left(\frac{KD}{K+k}\,I+\frac{k_BT}{K+k}\,e_0[1-E(L,K)]\right)\right.\\&\left.+\frac{k_BT}{K+k}\,[I-e_0LE(L,K)]\right],\end{aligned} \tag{A9}$$

in which

$$E(L,K)=\exp\left[-\frac{kL^2}{2k_BT}-\frac{K(D-L)^2}{2k_BT}+\frac{KD^2}{2k_BT}\right]. \tag{A10}$$

We introduce additional shorthand notation

$$f=\frac{KD}{K+k},\quad g=\frac{k_BT}{K+k}. \tag{A11}$$

A long calculation produces the second derivative

$$\begin{aligned}\frac{d^2I}{dK^2}&=\left(\frac{D}{k_BT}\right)^2\{f[fI+ge_0(1-E)]+g(I-e_0LE)]\}\\&-\frac{D}{(k_BT)^2}\,(f\{f[fI+ge_0(1-E)]+g(I-e_0LE)\}\\&-e_0L^2gE+2g[fI+ge_0(1-E)])\\&+\frac{1}{4(k_BT)^2}\,[f(f\{f[fI+ge_0(1-E)]+g(I-e_0LE)\}\\&-e_0L^2gE+2g[fI+ge_0(1-E)])-e_0L^3gE\\&+3fg[fI+ge_0(1-E)]+3g^2(I-e_0LE)],\end{aligned} \tag{A12}$$

in which we have simply expressed $E(L,K)$ by $E$. Because $D\gg L$, the maximum value for $K$ will be much less than $k$. Indeed, $K/k\sim L^2/D^2$. If we choose $D$ of order 300 nm with $L$ of order 10 nm, then $K$ is smaller than $k$ by three orders of magnitude. This makes $f\sim KD/k=L^2/D=L/30$. From Eq. (159), $I=3.75$ nm. Since $k=0.5$ gm/s$^2$, $g\sim k_BT/k=8$ nm$^2$. We have $fI=1.25$ nm$^2$. We now neglect $E$ compared to 1 and neglect $fI$ compared to $g$ and recall that $e_0=1$. This yields the approximations

$$\frac{dI}{dK}\cong\frac{D}{k_BT}\,g-\frac{1}{2k_BT}\,gI, \tag{A13}$$

$$\frac{d^2I}{dK^2}\cong\left(\frac{D}{k_BT}\right)^2gI-\frac{D}{(k_BT)^2}\,2g^2+\frac{1}{4(k_BT)^2}\,3g^2I. \tag{A14}$$

This time, the expression in large square brackets in Eq. (A3) yields

$$\begin{aligned}2C^2\left(\frac{dI}{dK}\right)^2-C(B+CI)\,\frac{d^2I}{dK^2}&\cong\frac{1}{(k_BT)^2}\,\{[2C^2D^2g^2-C(B+CI)D^2Ig]\\&-\tfrac{3}{4}(CBI+\tfrac{1}{3}C^2I^2)g^2\}.\end{aligned} \tag{A15}$$

From above, $I^2>g$, even for $K=0$, so that the first positive term on the right-hand side of Eq. (A15) is beaten by the second negative term. Thus the entire expression is negative. This makes the second flux derivative in Eq. (A3) negative as well. This explains the upper curve of Fig. 14 for the auxotonic load case.

[1] R. Brown, Philos. Mag. **4**, 161 (1828); Ann. Phys. Chem. **14**, 294 (1828).
[2] A. Einstein, *Investigations on the Theory of the Brownian Movement* (Dover, New York, 1956), with notes by R. Furth.
[3] B. J. Berne and R. Pecora, *Dynamic Light Scattering* (Wiley, New York, 1976).
[4] R. Nossal and H. Lecar, *Molecular and Cell Biophysics* (Addison-Wesley, Redwood City, CA 1991).
[5] L. Stryer, *Biochemistry*, 3rd ed. (Freeman, New York, 1988).
[6] T. Elston and G. Oster, Biophys. J. **73**(2), 703 (1997).
[7] C. S. Peskin, G. M. Odell, and G. Oster, Biophys. J. **65**, 316 (1993).
[8] A. F. Huxley, Prog. Biophys. Chem. **7**, 255 (1957); J. Physiol. (London) **243**, 1 (1974).
[9] (a) T. Mitsui and H. Oshima, J. Muscle Res. Cell Motil. **9**, 248 (1988); (b) M. Meister, S. R. Caplan, and H. C. Berg, Biophys. J. **55**, 905 (1989); (c) R. D. Vale and F. Oosawa, Adv. Biophys. **26**, 97 (1990); (d) N. Cordova, B. Ermentrout, and G. Oster, Proc. Natl. Acad. Sci. USA **89**, 339 (1991); (e) S. Leibler and D. Huse, C. R. Acad. Sci. III, **313**, 27 (1991).
[10] F. M. Harold, *The Vital Force: A Study of Bioenergetics* (Freeman, New York, 1986).
[11] C. de Duve, *A Guided Tour of the Living Cell* (Scientific American, New York, 1984).
[12] R. F. Fox, *Energy and the Evolution of Life* (Freeman, New York, 1988).
[13] R. Kubo, M. Toda, and N. Hashitsume, *Statistical Physics II* (Springer-Verlag, Berlin, 1985).
[14] D. E. Koshland, Sci. Am. **229**, 52 (1973).
[15] M. Karplus and J. A. McCammon, Annu. Rev. Biochem. **53**, 263 (1983).
[16] H. Frauenfelder, in *Structure and Motion: Membranes, Nucleic Acids, and Proteins*, edited by E. Clementi (Adenine, New York, 1985).
[17] R. Fowler and E. A. Guggenheim, *Statistical Thermodynamics* (Cambridge University Press, London, 1952), Sec. 1202.
[18] W. C. Gardiner, *Rates and Mechanisms of Chemical Reactions* (Benjamin, New York, 1969).
[19] D. Voet and J. G. Voet, *Biochemistry* (Wiley, New York, 1995).
[20] W. P. Jencks, in *Handbook of Biochemistry*, edited by H. A. Sober and R. A. Harte (Chemical Rubber Co., Cleveland, 1968), p. J-148.
[21] E. Eisenberg and T. L. Hill, Science **227**, 999 (1985).
[22] Transport ATPases, edited by E. Carafoli and A. Scarpa, Annals of the New York Academy of Sciences Vol. 402 (New York Academy of Sciences, New York, 1982).
[23] A. Lehninger, *Biochemistry* (Worth, New York, 1970).
[24] R. Cooke, CRC Crit. Rev. Biochem. **21**, 53 (1986).
[25] I. Rayment, H. M. Holden, M. Whittaker, C. B. Yohn, M. Lorenz, K. C. Holmes, and R. A. Milligan, Science **261**, 58 (1993).
[26] E. W. Taylor, Crit. Rev. Biochem. **7**, 103 (1979).
[27] W. T. Wicker, Science **266**, 1197 (1994).
[28] T. Elston, H. Wang, and G. Oster, Nature (London) ( to be published).
[29] P. D. Boyer, Biochim. Biophys. Acta **1140**, 215 (1993).
[30] C. S. Peskin and G. F. Oster, Biophys. J. **69**(6), 2268 (1995).